Nanostructured Materials for Pseudocapacitors and Single-Electron Devices

by

Long Pu

A thesis

presented to the University of Waterloo

in fulfilment of the

thesis requirement for the degree of

Master of Science

in

Chemistry – Nanotechnology

Waterloo, Ontario, Canada, 2014

Author's Declaration

I hereby declare that I am the sole author of this thesis. This is a true copy of the thesis, including any required final revisions, as accepted by my examiners.

I understand that my thesis may be made electronically available to the public.

Abstract

As a result of increasing demand of power in the modern society, energy storage/consumption is playing a more important role on future economics. Therefore energy storage systems which are more environmentally friendly, low-cost and high-performance have attracted much attention. Among electrochemical systems, supercapacitors are considered as a prominent candidate for the modern energy storage systems due to the high power density, high charge/discharge rate, and long lifetimes. Nevertheless, the performance of supercapacitors is limited by the significant disadvantage of low energy density. Metal oxides with high pseudocapacitance such as MnO_2 are used as the electrode materials for supercapacitors to resolve the lack of energy density in supercapacitors. The specific capacitance is notably enhanced by the metal oxides because of the reversible redox reactions. Previous studies confirmed that only a thin layer of MnO_2 is involved in the redox process and is electrochemically active, which makes surface area a critical factor of energy storage. To increase surface area of MnO_2, ZnO nanostructure is introduced in the electrode material as a template for electrodeposition of MnO_2. In the first part of the research, we synthesize a nanomaterial which combines 0-1-2 dimensional properties of different nanostructures and significantly increases the energy capacity of MnO_2.

In the second part of the research, we demonstrate an *in situ* synthesis of a hybrid device that combines two materials to investigate the individual characteristic of two nanomaterials. In this study, a ZnO nanorod interface on Au nanoparticle arrays is fabricated, and results in the photo-modulation of the array characteristics. We find the use of nanoparticle arrays as electrochemical systems by electrodepositing ZnO on Au nanoparticle arrays. The method expands their potential use in sensors, multifunctional materials, single electron transistors and nanoscale energy systems. Characteristic behavior of Au nanoparticle arrays including Coulomb blockade at room temperature, single electron charging effects and a power law dependence in current-voltage were observed, and Schottky behavior and photocurrent generation due to the ZnO nanorods were also proved. From the modulation of the threshold voltage of the Au array due to the electron-hole pairs generated by photo excitation in the ZnO rods, it can be seen that the system also has coupling between the Au nanoparticles and ZnO rods other than the individual characteristics. Au nanoparticles can be used as electrochemical systems with both structural and spatial confinement of the synthesized material. The possibility of using Au nanoparticle chains as electroactive sites significantly expands their potential use in sensors, multifunctional materials, single electron transistors and nanoscale energy systems.

Acknowledgements

I would like to express my special appreciation and thanks to my advisor Professor Dr. Vivek Maheshwari, for the continuous support of my study and research, for his patience, motivation, enthusiasm, and immense knowledge. His guidance helped me in all the time of research and writing of this thesis.

Besides my advisor, I would like to thank the rest of my thesis committee: Professor Juewen Liu and Professor Shirley Tang, for their encouragement, insightful comments, and hard questions.

I thank all my colleagues for their help during the research, they are Shehan Salgado, Abdulrahman Babatin, Abdullah Abbas, Maarij Baig, Huayi Gao.

Last but not least, I want to thank my wife Ou Wang and my family for their support.

Table of Contents

List of Figures

Chapter One-Nanomaterial combines 0-1-2 Dimensional Properties

1. Introduction

1.1 Purpose of the Study

Among electrochemical systems, supercapacitors have attracted much attention in recent years, due to their high power density, high charge/discharge rate, and long lifetimes. However, the limitation of low energy density is the bottleneck which holds back the applications of supercapacitors. The purpose of this study is to synthesize a composite material of MnO_2 and ZnO as a promising electrode material for supercapacitors. Electrodeposition of MnO_2 on ZnO nanostructure template benefits from high surface area and thus generates a much higher specific energy.

1.2 Statement of the Hypothesis

Specific capacitance of MnO_2 electrode material is increased by using ZnO nanostructure as a template during electrodeposition.

1.3 Significance of Study

Manganese dioxide is one of the most widely used electroactive materials in supercapacitors as a result of its abundant availability, environmental compatibility and high pseudocapacitance. However, previous research on

MnO_2 confirmed that the poor electrical conductivity and its strong thickness-dependent electroactivity are the major challenges. These defects limit the applications in electrochemical energy storage systems. To resolve the problems, this study focuses on electroplating of MnO_2 on a ZnO nanostructure template. The configuration not only speedups the redox reaction of MnO_2, but also significantly increases the surface area of MnO_2 by combining 0, 1 and 2 dimensional nanostructures. Therefore it produce a higher overall energy density compared to conventional MnO_2 electrode materials.

2. Literature Review

2.1 Supercapacitor

As a result of increasing demand of power in the modern society, energy storage/consumption is playing a more important role on future economics. The reliance on fossil fuels such as petroleum however has a severe impact on the global ecology. Therefore energy storage systems which are more environmentally friendly, low-cost and high-performance have attracted much attention[1]. Electrochemical energy storage/conversion system with the mentioned properties is a prominent candidate for the modern energy storage systems.

Electrochemical energy storage systems can be divided into three categories, which are batteries, fuel cells and supercapacitors, based on

different energy conversion mechanisms. The common denominators that the systems share are the separated electron/ion transport and that the energy conversion process happens at the electrode/electrolyte interface[1].

In batteries and fuel cells, energy is stored in the form of chemical energy and is converted to electrical energy through redox reactions[1]. Cathode, anode and electrolyte are the common components in both battery and fuel cell. Ionic conductivity is provided by electrolytes, which eventually allows electric charges move to move between two electrodes[1] (Figure 1, Figure 2).

The main difference between batteries and fuel cells is the locations where energy is stored[1]. In batteries, cathodes and anodes are the medium of charge-transfer and also the places energy is stored. Electrodes are either reduced or oxidized, thus the redox reaction powers the battery. As a closed system, energy storage and conversion happen inside the system which means chemical energy a battery carries is strictly limited to the electrode materials. On the contrary, fuel cells are open systems that require a constant source of chemical energy from outside the cell to run the reaction. Cathodes and anodes in fuel cells are just charge-transfer media. Because of the character, fuel cells are capable of producing electricity continuously if inputs are supplied constantly from environment.

In supercapacitors, electric energy is stored at the electrode/electrolyte interface where an electrochemical double layer is formed[2] (Figure 3). Energy

storage in the supercapacitors consists of electrostatic storage from separation of charge in a double layer at the electrode/electrolyte interface, and faradaic electrochemical storage from redox reactions.

An ideal energy storage system compromises high energy capacity and high rate of energy conversion. The reason for the interest in development of different electrochemical energy storage systems is shown in Figure 4, the so called "Ragone chart"[3]. It is a chart used for performance comparison of various energy storage and conversion devices. "Specific energy" (Wh/kg) or "energy density" (Wh/L) are the terms used to describe the energy contents of a system, whereas the speed of charge/discharge is indicated by the "specific power" (Wh/kg) or "power density" (Wh/L). The variations between the electrochemical energy storage systems come from the different energy storage/conversion mechanisms.

Fuel cells have the highest specific energy in the Ragone chart which is mainly because of the constant chemical energy source from outside. As the most widely used energy storage system, battery has a lower energy capacity compared to fuel cells. Capacitors can be considered as high power systems based on the charge/discharge mechanism. Supercapacitors occupy the area between batteries and conventional capacitors. It has several orders of magnitude higher power density than that of battery, with a higher amount of energy stored compared to a conventional capacitor. Nevertheless, the amount of energy stored in supercapacitors is significantly lower than that of

batteries and fuel cells. Therefore, the performance of supercapacitors is limited by the significant disadvantage of relatively low energy density: the amount of energy stored per unit weight is generally lower than that of a battery[4]. Supercapacitor which could store as much energy as batteries, but also with the outstanding feature of charge/discharge in minutes is considered an innovative device.

Supercapacitor was demonstrated and patented by General Electric in 1957[1]. Since then it has been attracting considerable attention from both scientists and engineers. With the features of longer cycle life, low maintenance, rapid charge/discharge and high power density, supercapacitors are believed to be capable of meeting the rapid growing demand for clean energy storage[5]. Nowadays, supercapacitors are used in a wide and growing range of high power density required applications.

Supercapacitors can be divided into two categories based on different energy storage mechanisms: electric double-layer capacitors (EDLCs) and pseudocapacitors[2]. EDLCs store energy using the adsorption of both anions and cations, and accumulated charge at electrode/electrolyte interface. So called “electric double-layer” refers to the layer of charge at the electrode/electrolyte interface that stores the charge. With the use of high surface area electrode materials significantly higher quantities of charge can be stored. Therefore, porous carbon materials with higher specific surface area (SSA) and pore-size distribution, such as activated carbons, aerogels,

xerogels, CNTs and mesoporous carbons, have been studied for use as electrodes in EDLCs[2]. As a result of electrostatic surface-charge accumulation, EDLCs have very high rates of charge/discharge and infinite lifetime in principles which makes it environmentally friendly (Figure 5).

On the other hand, pseudo-capacitors store energy through Faradic reduction-oxidation reactions[5]. Large pseudo-capacitance comes from charge transfer between electrode and electroactive materials where there is fast and reversible chemical reactions taking place on the electrode surface (Figure 6). Two types of electroactive materials that exhibit high pseudocapacitance have been investigated widely: 1) conducting polymers, including polyaniline, polypyrrole and polythiophene, 2) transition metal oxides, such as manganese oxide and ruthenium oxide[4]. Pseudocapacitance-based devices can store more energy compared to EDLCs because of the higher charge storage from the Faradic reaction mechanism. Nevertheless, power density is limited by the poor electrical conductivity of these electroactive materials, and the relatively slow response time of the chemical redox reaction. Easily damaged structure during the redox process results in a relatively poor electrochemical stability compared to EDLCs.

The overall performance of a supercapacitor is contributed by electrostatic capacitance from the double layer and pseudocapacitance from redox reactions. Thus electrode material is the key component in an electrochemical capacitor because it determines the system's capacity. My

research is to synthesis a composite material of MnO_2 and ZnO as a promising electrode material for pseudocapacitors.

2.2 Manganese Dioxide

Transition metal oxides have been investigated as electroactive materials for a long time[6]. Ruthenium and iridium oxides were initially investigated but iron and manganese oxides are drawing more attention recently because of their low cost and low toxicity. Manganese dioxides have been used as electrode material in traditional alkaline battery, and it is also used in the newer lithium-ion batteries in the spinel $Li_{1+x}Mn_2O_4$ form[7]. Due to the good pseudocapacitance, application of MnO_2 as continued to expand to supercapacitors. Amorphous MnO_2 was initially incorporated into composite electrode structure and exhibited a capacitor-like electrochemical response. Since then, research interest on MnO_2 as an electroactive has grown steadily, as a result of its abundant availability and environmental compatibility[7].

The performance of MnO_2 in supercapacitors is determined by its surface area and electric conductivity. Because of the poor electric conductivity of MnO_2, a nanoscale thin MnO_2 film or coating on the current collector overcome the limitations on the conductivity and also increase the surface area. Recent trend of coating MnO_2 nanostructure on the surface of 3-dimensional porous carbon nanomaterials, gives specific capacitances as high as 400-600 F/g[8].

In order to understand the factors that control the charge-storage process and to improve the performance of MnO_2 electrode material, a detailed knowledge of the charge-storage mechanism is important. A mechanism based on the surface adsorption of electrolyte cations (C^+) on MnO_2 was proposed to explain the charge storage behavior of pseudo-capacitance in MnO_2[7] (equation 1). In presence of cations from electrolyte, Mn stores electric charge, and the oxidation state of Mn changes from +4 to +3.

$$MnO_2 + C^+ + e^- \leftrightarrow MnOOC \quad (1)$$

where $C^+ = Na^+, K^+, Li^+$.

Previous studies also confirmed that a thin layer of MnO_2 is involved in the redox process and is electrochemically active[7]. Whereas no change of the Mn oxidation states is observed for thick bulk material which contains the same amorphous MnO_2. The charge-storage mechanism makes surface area a critical factor that determines the performance of MnO_2 as a supercapacitor electrode material[8].

Recently, nanostructured materials with novel electrical, optical, magnetic and mechanical properties have attracted significant amount of attention. Therefore, instead of using bulk conventional material, a thin layer of MnO_2 nanoparticles are used in our study to optimize the performance. A nanostructure template for the growth of MnO_2 would benefits the energy capacity of the composite material by increasing surface area[9,10].

2.3 Nanomaterials

While reduction in size, nanomaterials with distinct chemical, mechanical and electrical properties have attracted much attention since the development of nanotechnology. Research on nanomaterials show that unique properties are derived from different dimensional structures[11].

For a better understanding, classifications for nanomaterials are made based on the number of dimensions of a material which are not confined to the nanoscale range (<100 nm). Zero-dimensional (0-D) represents materials in which all the three dimensions are confined within the nanoscale (Figure 7). Nanoparticles no larger than 100 nm are good examples of 0-D nanomaterials. 0-D nanomaterials can be amorphous, single crystalline or polycrystalline. Various shapes and form are found for nanoparticles, for example nanoclusters, nanospheres and nanodispersions. Nanowires, nanorods are the common 1-D nanomaterials, which have 1 dimension outside the nanoscale. This results in needle-like shapes for 1-D nanomaterials, and the lengths of different materials varies from 100 nm to tens of micrometers. Sheet-like 2-D nanomaterials are formed when two of the dimensions are not confined to the nanoscale. 2-D nanomaterials have various forms, such as nanofilms, nanosheets and nanonetworks. Three dimensional nanomaterials have no dimension confined to the nanoscale, 3-D nanomaterials can be composed of a multiple arrangement of nanoscale crystals in different orientations. Dispersions of nanoparticles, bundles of nanowires as well as multiple nanosheets closely contact with each other also form 3-D nanomaterials.

Because of their unique mechanical, electrical, optical and magnetic properties, nanomaterials have attracted much attention recently[12]. Inorganic nanowires and nanorods can be used in optoelectronics as a result of their interesting optical and electrical properties[11,13]. Their tunable size and shape through synthesis lead to tunable properties and make them favored in specialized applications. Nanoparticles have been also studies as the bridge between conventional bulk materials and atomic structures. In a bulk material, physical properties are observed constant despite of size, whereas size-dependent properties are observed in nanomaterials.

2.4 Zinc Oxide

Zinc oxide has a chemical formula of ZnO, which is a water-insoluble white powder. ZnO has been widely used applications such as: dye-sensitized solar cells, transparent electrodes and batteries.[14] The compound of ZnO can also be found as a mineral zincite in the environment. As a wide band gap semiconducting metal oxide, ZnO has attracted attention in the research community for a long time. The high electron mobility of ZnO makes the semiconductor a good material for current collectors in dye-sensitized solar cells[15]. Since the development of nanotechnology in recent years, unique properties have been observed in ZnO nanostructures. Research also confirmed the growth of zinc oxide nanoneedles, nanorods, nanosheets and nanorings[15,16]. Synthesis of nanostructure ZnO can be accomplished through various techniques including chemical vapor deposition, thermal evaporation and electrodeposition[16], etc.

Crystal Structure

In material science, hexagonal wurtzite and cubic zincblende are the two main crystal structures for most of the II-VI group binary compounds[14]. Because oxygen is a member of IIA group and zinc is classed into IIB group, the II-VI group semiconductor ZnO also share the hexagonal wurtzite (Figure 8) and cubic zincblende (Figure 9) structures, along with the rare rocksalt structure obtained at relatively high pressures[16].

Wurtzite is the common structure for ZnO because it is the most thermodynamically stable phase at ambient conditions. It has a hexagonal structure (space group C_{6v})[16]. Two lattice constant are a = 3.29 Å and c = 5.2 Å, and the c/a ratio is 1.6 which is close to the ideal ratio (1.633). The wurtzite structure can be understood as alternating Zn^{2+} and O^{2-} tetrahedracally coordinated ions, stacked alternately along the c-axis. In each tetrahedron sublattice, every atom of one kind is surrounded by four atoms of other kind. With the corresponding radii of 0.074 nm for Zn^{2+} and 0.140 nm for O^{2-}, the largely ionic ZnO bonding is the reason for preferential formation of wurtzite rather than other structures.

The metastable zincblende crystal structure is only stabilized by growing ZnO on cubic lattice substrates.[14] Two interpenetrating face-centered-cubic sublattices shift along the body diagonal by one quarter of a body diagonal in the zincblende structure. Tetrahedral sublattices appear in both wurtzite and zincblende crystal structures, and is found to be the

characteristic geometry for zinc. The different stacking sequence of closed-paced planes is the main difference between two structures.

No inversion symmetry exists in the main forms of ZnO, gives the semiconductor another important property-piezoelectricity[15]. Piezoelectricity is defined by the electric charge accumulation when a strain is applied to a material. Because of the atomic scale polarization, an electric dipole is generated and a linear electromechanical interaction was observed with respect to the strain applied. Being able to convert a mechanical stress to an electric signal, materials show piezoelectricity property are widely used in high voltage and power sources and sensors[14]. A comparable high piezoelectric tensor to that of GaN and AlN results in a wide application of ZnO materials.

Electrical Properties

A relatively wide bad gap of 3.37 eV at 300 k is one of the main reasons of expanding academic interest on ZnO materials[17]. The band gap can be further enlarged by alloying ZnO with MgO or CdO. A wide band gap brings several advantages to a semiconductor material, such as higher breakdown voltages, lower electronic noise, and ability to sustain large electric fields.

To understand the electron transportation in semiconductors, two situations are considered. When a low electric field is applied to a semiconductor, the energy gained from the electric field is not enough compared to the excitation energy of electrons, hence the energy distribution

of electrons is not affected by the low electric field. Electron mobility which is determined by the electron distribution function therefore stays the same. While the external electric field is high enough that the energy gained by electrons are no longer negligible compared to the thermal energy of the semiconductor electrons, electron distribution function is changed because of the energy obtained. Compared to amorphous silicon or organic semiconductors, ZnO has a relatively high electron mobility with a room temperature value of 205 $cm^2/(V\ s)$ and a maximum value of ~2000 $cm^2/(V\ s)$[14,16].

Various ZnO nanostructure have been fabricated and most of them have n-type character, because of native defects such as oxygen vacancies and zinc interstitials[16]. Other than the intrinsic character, n-type doping can also be achieved by substituting Zn with group-III elements or by substituting O with group-VII elements. However, difficulty of p-type doping on ZnO is the still a major impediment. The main reason is the low solubility of p-type dopants and their compensation by abundant n-type impurities[15]. Several p-type doping with GaN and ZnSe have been reported[17].

ZnO Nanostructure Synthesis

ZnO is one of the few remarkable semiconducting and piezoelectric materials that form self-assembled nanostructures in specific orientations. Well-defined ZnO nanostructures, such as nanowires, nanorods, nanoplates, and nanorings have been successfully synthesized using different methods. Because of their

interesting optical and electrical properties, oriented nanostructures are preferable in numerous applications.

ZnO nanostructure can be synthesized by using different methods, such as vapor transport, wet chemical process, pulsed laser deposition, etc[14,16]. Although electrodeposition is not the dominant synthesis method, it presents a cost-effective method to prepare ZnO nanostructures at low temperatures under normal laboratory conditions[16]. The shape and growth orientation of nanostructure can be precisely controlled in electrodeposition. The presence of chemically dissimilar lattice faces can be selectively bound by capping agents, which result in different surface energies and growth mechanisms[18,19].

The most thermodynamically stable structure wurtzite is described as a number of alternating planes composed of tetrahedracally coordinated O^{2-} and Zn^{2+} ions, stacked alternatively along the c axis. The typical crystal structure shows a negatively charged basal plane $(000\bar{1})$ which is occupied by oxygen ions, and a top positively plane (0001) occupied by zinc ions (Figure 10). Other than the top and basal polar planes, the low-index faces which are parallel to the c-axis consist a nonpolar $(10\bar{1}0)$ plane[18,20].

ZnO Nanorods

During the electrochemical deposition of ZnO nanostructure, the crystal growth along c-axis is favored. The reason for preferentially growth along <0001> direction is electrostatic deposition of zincate ion ($Zn(OH)_4^{2-}$) onto the (0001) plane. $Zn(OH)_4^{2-}$ ion has been reported as the growth unit of ZnO

nanostructure in aqueous solution[14,18]. When the negatively charged zincate ions are adsorbed on the positive polar face of (0001) by electrostatic force, the anisotropic growth of the crystal along the <0001> direction is allowed.

ZnO Nanosheets

Thin nanosheet is desirable as a 2-D nanomaterial with unique properties. To synthesis ZnO nanosheets, the preferential growth direction must be altered during the electrodeposition. Capping agents can be used to selectively bind specific crystal planes, therefore the shape and growth mechanisms can be precisely controlled[18,20]. By investigating the crystal structure of ZnO, it can be seen that the growth along c-axis needs to be hindered so growth in other directions are favored. The growth mechanism can be achieved by adding KCl as a supporting electrolyte to the aqueous solution[19]. When KCl is added, the negatively charged Cl^- ions are preferentially adsorbed on the positive polar face of (0001) surface. The electrostatic adsorption further prevents the contact of $Zn(OH)_4^{2-}$ onto the top surface, and limits the growth along the c-axis. Therefore leads to a preferential growth on the $(10\bar{1}0)$ plane, the hexagonal shape of the ZnO is expanding while the thickness is not growing result in the formation of ZnO nanosheets.

Large charge density is accumulated at the edges of the nanosheets during the electrochemical process. The electrostatic repulsion force between the ZnO nanosheets pushes the sheets to stay away from each other at the

edges. The Coulomb force thus leads the out-of-plane growth which is vertical to the substrate[18,21] (Figure 11).

Figure 12 is a schematic of the research. ZnO nanosheets are firstly deposited on an Indium tin oxide (ITO) coated glass substrate, then ZnO nanorods are electrodeposited on the surface of the nanosheets. A thin layer of MnO_2 nanoparticles are finally deposited on the ZnO nanostructure. Thin films of Au are sputtered between each step to increase the charge collect capacity and work as current collector. Because of the high surface area of the ZnO substrate and the high electric field at the tips of the nanorods, the specific capacitance of the material will be increased as well as the speed of redox reaction on MnO_2.

3. Methodology

3.1 Instrumentation

CompactStat was used for the electrochemical deposition and also for the cyclic voltammetry (CV) measurements. It is a portable electrochemical interface & impendence analyzer from IVIUM Technologies.

Field emission scanning electron microscopy (FE-SEM) was used to evaluate morphologies of the samples. Imaging were taken ULTRA PLUS by Carl Zeiss.

3.2 Experimental Procedures

Preparation of Substrates

ITO coated glasses were used as substrates for hierarchical growth of ZnO nanostructure. The substrates with sheet resistances of about 12 ohm were obtained from Delta technologies. To wash the ITO substrate, it was first rinsed by Millipore water, and then it was left in a 1:10 diluted detergent solution, a 1:1 mixture of acetone and isopropanol and Millipore water in sequence for sonication. Each sonication lasted for 10 minutes. Finally, the substrate was dried under a nitrogen gas stream.

Hierarchical Electrochemical Deposition of ZnO Nanostructure

The electrochemical deposition of ZnO nanosheets, nanorods and MnO_2 nanoparticles were carried out by using CompactStat. Standard three electrode setup was used during the depositions (Figure 13). A Ag/AgCl electrode was used as the reference electrode, and a platinum wire was connected to the counter electrode for all the depositions. Different substrates were connected to working electrode during each step of electrodepositions.

The electrochemical depositions of ZnO nanosheets were done on ITO coated glass substrates. A clean substrate was used as the working electrode and a constant electric potential difference of -0.955 V was applied for 2000s. 0.05 M $Zn(NO_3)_2$ with 0.06 M KCl aqueous solution was used as electrolyte for the electrochemical deposition. A beaker filled with electrolyte solution was immersed in a silicon oil bath which was heated on a hot plate,

to maintain a steady temperature of 75 ℃ during the electrodeposition. Substrates were washed thoroughly with Millipore water after the deposition to remove the excessive electrolyte and dried under a nitrogen stream. The substrates were then heated at 350 ℃ for two hours for the annealing of ZnO nanosheets.

Before the second deposition of hierarchical ZnO nanorods on the surface of nanosheets, a thin layer of gold was sputtered on the surface of ZnO nanosheet to improve the charge collection capacity. The substrate was then used as the working electrode. Same voltage of -0.955 V was applied to the working electrode for the same amount of time at same temperature as in the first step. A lower concentration of 0.005 M $Zn(NO_3)_2$ aqueous solution was used as the electrolyte. After the deposition, the substrate was again washed thoroughly with Millipore water and then dried under a nitrogen stream. Two hours of annealing at 350 ℃ was applied to stabilize the ZnO nanostructures.

Electrochemical Deposition of MnO_2

To electrochemically deposit a film of MnO_2 on ZnO nanostructure template, a thin layer of gold was sputtered again on the substrate that has ZnO nanostructures. The substrate was immersed into a plating solution of 20 mM $Mn(NO_3)_2$ with 100 mM $NaNO_3$. A constant current of 100 $\mu A/cm^2$ was applied for 5 minutes. The substrate was washed with Millipore water after

the deposition to remove excessive electrolyte, and then dried on a hot plate at 60 ℃ for 2 hours.

3.3 Sample Testing Procedures

The primary limitation on application of supercapacitors is the lack of energy density. As a key component in a supercapacitor, the electrode material plays an important role on determining the capacity of a supercapacitor. Therefore a crucial metric for an electrode material is its specific capacitance. Standardized measurement methods are used to evaluate the performance of a material as an electrode material in supercapacitors.

Test Fixture Configuration

In a typical supercapacitor unit cell, two electrodes are separated by a porous separator, which prevents electric charge flow but allows ionic current to flow between the two electrodes. We used a test fixture configuration that mimics the standard unit cell to estimate the electrode material. A two-electrode configuration was used to analyze the electrode material. In this setup, two substrates coated with same material were used as symmetrical electrodes and a porous paper was used as the separator. The setup was fixed by two metal plates and is immersed in an electrolyte solution of 1 M KCl (Figure 14).

Measurement Procedures

To test the capacity performance of the nanomaterial combines MnO_2 and ZnO, cyclic voltammetry measurements were carried out by using CompactStat. The range of the testing was 0-0.8 volts, which is a standard

voltage range for MnO_2 containing materials. From a CV plot, capacitance for the two-electrode cell can be measured[22,23].

$$C = I/(dV/dt) \quad (2)$$

This equation determines the capacitance of the two-electrode cell, however it is more important to assess the performance of the electrode material. Specific capacitance is defined as the capacitance per unit mass (area, volume) for a material. The equation blow is used to accurately calculate the specific capacitance.

$$C_{sp}\left(\frac{F}{cm^2}\right) = 4 \times C/A \quad (3)$$

Specific capacitance per unit area is calculated for the nanomaterial composite because it gives a better understanding on the material than specific capacitance per unit mass. A in the above equation is the total surface area of the active material on both electrodes. The multiplier of 4 is used because it adjusts the overall capacitance of the two electrode cell and the total surface area on both electrodes to the specific capacitance per unit area of one single electrode.

4. Results

4.1 Zinc Oxide Nanostructure

Figure 15 is a FESEM image of ZnO nanorods when 0.005 M $Zn(NO_3)_2$ was used as the electrolyte in the electrochemical deposition. The nanorods have

the typical hexagonal structure which is expected from the wurtzite crystal lattice with a diameter around 100 nm.

When the concentration of $Zn(NO_3)_2$ was increased to 0.05 M while all the other parameters stay the same, we got thick nanoplates instead of nanorods. It can be seen from the FE-SEM image (Figure 16) that the thickness and diameter of the ZnO nanoplates are both around 1 μm. Nanoplates with thickness in the range of micron does not fit the need of electrode material as the surface area is not improved compared to planar surface.

To make thinner nanosheets, KCl is added to the aqueous solution as a supporting electrolyte. Adsorption of Cl^- ions onto the (0001) surface prevents the adsorption of zincate ions, thus hindered the growth along c-axis. Figure 17 shows the growth of ZnO is preferred in other directions while the growth in thickness which is c-axis is blocked. The ZnO nanosheets are thinner than 100 nm and as wide as 4 μm.

During the hierarchical electrochemical deposition of ZnO nanostructure, the nanosheets were deposited on ITO substrates, followed by the deposition of ZnO nanorods. From the FE-SEM image (Figure 18), we can see that nanorods are growing on both sides of the sheets with the hexagonal shape.

4.2 Manganese Dioxide Deposition

MnO_2 nanoparticles were electrochemically deposited on the ZnO template. To coat only a thin layer of MnO_2, different growth time were used for comparison. Figure 19 and Figure 20 show the MnO_2 growth for 5 minutes and 20 minutes respectively. Compared to the ZnO nanostructure without MnO_2, the blur in Figure 19 is primarily caused by the poor electrical conductivity of MnO_2, while the hexagonal shape can still be seen. However when the growth lasted for 20 minutes, the ZnO nanostructure template was completely covered by a thick layer of MnO_2. The reason MnO_2 nanoparticles were only grown for 5 minutes instead of longer time is that to maintain the structure of ZnO template. Longer time growth would have the same result as growing MnO_2 on thick nanoplates. Therefore to benefit from the high surface area and high electric field, MnO_2 nanoparticles were grown for 5 minutes.

Energy-dispersive X-ray spectroscopy (EDS) was also used for the chemical characterization of the sample. Oxygen, zinc, gold and manganese peaks were observed in the EDS spectrum (Figure 21), and the Mn growth is confirmed. Mn peak was lower than that of other elements, which is expected because the nanoscopically growth of MnO_2 thin layer.

4.3 Electric Behavior

Cyclic voltammetry was carried out to determine the energy capacity of the nanocomposite material. Figure 22 shows the CV measurements on the

material at different scan rates. The scan rate started from a low speed of 10 mV/s and increased to 200 mV/s. Different scan rates were performed to evaluate the ability of the material to work under various scan speed. It can be expected that the shape of the cyclic voltammetry is getting better or more ideal as a rectangle when the scan rate decreases. Because at lower scan rates, there is a sufficient time for the redox reaction on the electroactive material to happen. Thus at higher scan rates, the electrode material functions more like a resistor. To measure the capacitance based on an average value, the specific capacitance of the nanocomposite material was calculated using the CV at a standard scan rate of 50 mV/s. With a surface area of 2.2 cm^2 on each ITO, the specific capacitance is calculated to be 26.2 mF/cm^2 using equation 2 and 3.

Lifetime is another important factor for electrochemical energy storage systems. To test the cycle life, CV was repeated for 100 times at 50 mV/s on the nanomaterial. Figure 23 shows the decrease of specific capacitance in 100 cycles. A decrease was observed from 26.2 mF/cm^2 to 24.2 mF/cm^2, which is around 7.5% of the original capacitance.

A control was made to accurately evaluate the improvement in specific capacitance by electrodepositing MnO_2 on a plain ITO substrate for 5 minutes. Other than that, a series of samples were also made to confirm the increase in specific capacitance comes from the increase in the surface area of

MnO_2.Figure 24, Figure 25 and Figure 26 are FESEM images of 5 minutes growth of MnO_2 on ITO, ZnO nanorods and ZnO nanosheets respectively.

Figure 27 is the CV comparison for different samples, and a significant increase in the current level from the sample with MnO_2 on ITO to the sample with MnO_2 on ZnO nanostructure was observed. Table 1 is a conclusion of the specific capacitance values of different samples. From the planar surface to the ZnO nanostructure template, the specific capacitance increase from 2.77 mF/cm^2 to 26.2 mF/cm^2 (Table 1). Because ZnO is not a good electroactive material, the 9.5 time increase in specific capacitance is mainly from the increase in the surface area of MnO_2.

5. Conclusion

5.1 Summary of Findings

By electrodeposition of MnO_2 onto the ZnO nanostructure template, a 9.5 times increase in the specific capacitance per unit area was observed. The nanocomposite material benefits from high surface area on the ZnO template and thus generates a much higher specific energy compared to plain MnO_2 on a planar substrate. The material can be used as a promising electrode material for pseudocapacitors.

5.2 Future Research

Because we are still at an early stage of the research, more characterizations of the nanocomposite material need to be done to evaluate the performance of the material for potential use in practical applications.

To accurately measure the increase of surface area in the nanocomposite, Brunauer-Emmett-Teller (BET) theory can be used. The BET method is based on adsorption of gas molecules on a solid surface. Hence exact surface area will be determined depend on the amount of gas adsorbed at a given pressure.

Quantification of MnO_2 nanoparticles is an important aspect for the future research. Because of its charge storage mechanism, it is crucial to have a high surface of MnO_2 and also have only a thin layer of MnO_2 nanoparticles on the substrate simultaneously. MnO_2 was grown for only 5 minutes in the

experiments, and we have not done any quantification on the MnO_2 nanoparticles. Either the time of deposition or the current applied on the system can be varied solely, or altered at the same time. The best amount of MnO_2 coated on the ZnO nanostructure template should comprise not only a good coverage on each and every ZnO nanorod but also a good thickness of the MnO_2 layer.

As a remarkable semiconducting oxide that forms self-assembled structure in specific orientations. There are many potential hierarchical nanostructures of ZnO other than nanorods on nanosheets. Therefore it is possible to find another ZnO nanostructure that contributes even more surface area. Or we can simply make modifications to the ZnO nanostructure that we have, for example, varying the densities and the diameters of the nanosheets and the nanorods. Another approach would be increasing the length of the nanorods to an extent that the nanorods are long enough to connect two nanosheets. By doing that 3-D nanomatrix or nanonetworks will be formed.

Finally, more electrical characterization needs to be done to the final nanomaterial. Galvanostatic or constant current charge/discharge curves also gives a good understanding on the energy density of the material with minor errors. On the other hand, a model can be developed to calculate the 'ideality' of a cyclic voltammetry curve. This can be done by calculating the average absolute deviation of each data point, and the result would tell how good the cyclic voltammetry is compared to a rectangle.

Chapter Two-Hybrid Device of Nanoparticle Chains Couples to Semiconducting Rods

1. Introduction

1.1 Purpose of the Study

The purpose is to show that Au nanoparticle arrays can be used as electrochemically active systems and used to assembly nanomaterials.

1.2 Statement of the Hypothesis

Hybrid devices consisting of distinct nanomaterials can be constructed with spatially confined geometry. The hybrid devices should also show a behavior that combines the individualistic characteristics of the each nanomaterials that is part of the device.

1.3 Significance of Study

A board range of electric behavior have been observed for nanoparticle arrays formed by nanoparticles, such as Coulomb blockade, Coulomb staircase, change in conductivity from conductors to insulators, and sensitivity to gating. Because of single electron charging effect, quantum confinement and coupling between adjacent nanoparticles, room temperature Coulomb blockade and single electron behavior are observed. To further investigate the characteristic properties of the nanoparticle arrays, other nanomaterials are attached to the arrays. Mutual modulation on electrical behaviors between

two distinct nanomaterials are studied. The interface of nanoparticle arrays and nanomaterials will be useful in applications such as nanoscale electro-optical devices, electrochemical sensors, nanoscale energy storage systems.

2. Literature Review

2.1 Nanoparticle and Their arrays

Because of the potential of low power operation involving only a few electrons, single electron transistors have come to be considered candidates for future integrated circuit[24-26]. Even the replacing of silicon transistors by single electron devices does not happen, single electron devices play a crucial role in fabrication of size limiting electronic devices. Since the manipulation of nanoparticle and their arrays, an approach of single electron devices has been achieved. Various electric behavior have been observed in nanoparticle arrays, such as Coulomb blockade, Coulomb staircase, change in conductivity from conductors to insulators, and sensitivity to gating[24,26,27]. These properties stem from single electron charging, quantum confinement, and neighboring particles coupling. Nonetheless, even for a single layer of metal nanoparticles, some aspects of the electric behavior remain poorly understood[27].

By understanding and modelling nanoparticle and their arrays, they can be tailored and used in new devices and sensors. Incorporate nanomaterials

with the nanoparticle arrays gives multifunctional materials which lead to applications require characteristic properties[24].

As one of the interesting phenomena, Coulomb blockade is the increased resistance at small bias voltages. In a single electron transistor, Coulomb blockade happens when Coulomb repulsion between electrons increases the energy, thus electrons pass through the system one-by-one, and in some cases the current is suppressed at low temperature and low voltages. As a result, the resistance of the device is not constant at low bias voltages and increase to infinity under the threshold voltage.

2.2 Au Nanoparticles

Gold has been investigated as one of the ancient topics. Recently, new gold materials such as Au nanoparticles and self-assembled monolayers are drawing increasing attentions. Au nanoparticles are considered stable metal nanoparticles. With the compelling properties, such as optical features, size-related electronic and multiple assembly types, Au nanoparticle is a rising candidate as building block in the bottom-up approach, and has been used in electro-optical devices and sensors[28].

There are various ways of fabricating Au nanoparticles, however citrate reduction introduced in 1973 is the most popular method. Au nanoparticles are made using citrate reduction of a gold (III) derivative-$HAuCl_4$ in this method, and the size of nanoparticle can be controlled by varying the citrate-to-gold ratio[28]. For example, 0.01 % citrate, < 0.1 % Au

and > 99 % water would result in an average size of 10 nm Au nanoparticle in solution.

To investigate the individual characteristic of two nanomaterials, we demonstrate an *in situ* synthesis of a hybrid device that combines two materials. Figure 28 shows a schematic of our hybrid device. Au nanoparticle arrays are represented by the underlying red dots and the purple rods are ZnO rods growing on the arrays.

3. Methodology

3.1 Instrumentation

Ultraviolet-visible spectroscopy was carried out by using MINI-D2T deuterium tungsten light source and USB2000 Miniature fiber optic spectrometer from Ocean Optics.

Current-Voltage (I-V) response was measured by 3458A Digital multimeter from Agilent Technologies, while the circuit is powered by 6614C 50 Watt system power supply from the same company.

Newport 69907 Universal arc lamp power supply delivers power to the lamp and worked as the solar simulator in our experiments.

3.2 Experimental Procedures

Preparation of Gold Chips

Gold chips were designed for the testing purpose as a substrate device. It is a silicon substrate with a 200 nm thick SiO_2 layer on top of it. Above the SiO_2, there are 110 Au electrodes and one ground (Figure 29). In the center of the chip, alternating fingers from the Au electrodes and the ground form a morphology of 5 μm wide Au pads separated from 2 μm wide gaps. The SiO_2 gaps are the places where we did the synthesis. Gold chips were washed with Millipore water first, and then sonicated in a 1:1 mixture of acetone and isopropanol for 10 minutes, followed by another 10 minutes sonication in Millipore water. Piranha solution was used to clean organic matter off the gold substrate, and also to make the gold chip hydrophilic for later deposition of Au nanoparticle chains. Gold chip was washed thoroughly with Millipore water after being immersed in the piranha solution for 3 minutes. The purpose of piranha solution was to add OH groups to the SiO_2 surface. A 1% (3-Aminopropyl) triethoxysilane (APTES) solution was made by diluting 200 μL APTES to 20 mL total solution using Millipore water. The gold chips were left in the solution for 10 minutes, and this step further functionalizes the SiO_2 surface with amine groups by replacing OH groups. The electrostatic force between the amine groups on the SiO_2 surface and Au nanoparticles later motivates the deposition of Au nanoparticles. The chip was dried and then left on a hot plate at 150 ℃ for 30 minutes.

Preparation of Gold Nanoparticle Chains

Gold nanoparticles were purchased from BBI solutions. The nanoparticles with around 10 nm in diameter are stably suspended in water with deep red in color. All the glass vials, caps, pipette tips and Millipore water were autoclaved to sterilize the equipment for elimination of any possible contaminants. 360 µL of 1 mg/mL $CaCl_2$ was added to a glass vial which contains 4.0 mL of the stock Au nanoparticles. The final solution was put on a vortex mixer for eight hours for assembling of Au-nanoparticles. While the 10 nm Au nanoparticles were cross-linked with the Ca^{2+} ions to form larger nanoparticle chains, the solution mixture became blue in color. The color change was caused by surface plasmon resonance (SPR): oscillating electric field of a light ray interact with the free electrons near a colloidal nanoparticle, leads to a concerted oscillation of electron charge resonance with the frequency of visible light. The SPR causes an adsorption of light in the blue region and results a red color for small nanoparticles. When particle size increases, the wavelength of the SPR adsorption shifts to longer wavelengths and blue light is reflected.

Deposition of Au Nanoparticles on Au Chips

Au nanoparticle arrays were passively deposited on the SiO_2 between two gold fingers on a Au chip. The chip was deposited in the solution of Au nanoparticle chains for 1 hour, with the side to be deposited facing up. After 1 hour, Au chip was taken out from solution and rinsed indirectly by squeezing

Millipore water to the tweezers which is holding the Au chip. Excessive Au nanoparticles should have been washed away from the Au chip.

Electrochemical Deposition of ZnO Nanorods on Au Nanoparticle Arrays

ZnO nanorods were electrochemically deposited on the Au nanoparticle arrays. Firstly, the patterned substrate with Au nanoparticle arrays was fixed in a microfluidic cell. The cell was designed in a way that aqueous solution can be stored only in the center part, and leaves the edges of the Au chip away from the aqueous solution. Therefore the Au electrodes can still be accessed through the outside end of the electrodes. An aqueous solution of 1.25 mM $ZnCl_2$ and 0.1 M KCl was used as the electrolyte, and a potential difference of -0.955 volts was applied for 420 seconds. The electrochemical deposition was done by using a typical three-electrode setup, where the working electrode is connected to the Au electrode that we want to grow ZnO on. A standard silver-chloride electrode was used as the reference electrode and immersed in the solution and a platinum wire was connected to the counter electrode end (Figure 30). After the deposition, the Au chip substrate was rinsed with Millipore water and heated on a hot plate at 150 ℃ for 30 minutes.

4. Results

4.1 Au Nanoparticles Chains

By using Ca^{2+} ions, Au nanoparticles were self-assembled to nanoparticle arrays. It can be observed in UV-Vis that the absorption peak shifted from 525 nm for the red Au nanoparticles to around 600 nm for the blue Au nanoparticle chains (Figure 31). The change in nanoparticle size was studied by using dynamic light scattering (DLS). Before the addition of calcium ions, the size of nanoparticles is ~10 nm. A significant increase in size was observed after the mixing of Ca^{2+} ions with Au nanoparticles. Zeta potential was also measured before and after the formation of nanoparticle arrays. A constant value of ~-40 mV shows the limitation of zeta potential on the formation of nanoparticle chains. To further confirm the formation of nanoparticle arrays, a typical chain structure formed by Au nanoparticles was observed in Transmission electron microscopy (TEM) (Figure 32). The lengths of nanoparticle arrays were in the range of microns, and the spacing between nanoparticles was measured to be 1-2 nm.

The FE-SEM image clearly shows the Au nanoparticle arrays which connect two Au electrodes (Figure 33). From the typical current-voltage response, the characteristic Coulomb blockade with a threshold voltage V_T was observed, and negative differential conductance showing in the inset of Figure 34 is a result of the single electron charging effects[25,26]. Further investigation on the I-V response can be fitted to a power law model, with a

threshold voltage of 4.87 volts and a power law scaling with 2.6. The room temperature Coulomb blockade are caused by the defects such as single Au nanoparticle pathway in Figure 33, which obeys the electric conduction through 2-D arrays of nanoparticles.

4.2 ZnO Nanorods on Au Nanoparticles

Figure 35 is a FESEM image shows the ZnO nanorods growth on Au nanoparticle chains after the electrodeposition. Inset of this figure shows the same location before the growth of ZnO nanorods, where we only had the Au nanoparticle arrays. ZnO nanorods are proved to grow only on the Au nanoparticle chains with diameters between 20-30 nm. Figure 36 shows the typical hexagonal shape of ZnO rods and Figure 37 shows the underlying Au particles which can be seen as bright silhouette. The ZnO nanorods match well with the size of the Au nanoparticle chains, which means that Au nanoparticles act not only as conducting pathways in the electrochemical deposition, but also preferential growth sites for ZnO nanorods.

4.3 Characterization of Hybrid Device

The hybrid device consisting of ZnO nanorods and Au nanoparticles was characterized for its current-voltage response and photo excitation properties (Figure 38). From the I-V response under dark conditions, oscillations in the differential conductance suggest the conduction of electric current through the Au nanoparticle pathway underneath ZnO nanorods (inset of Figure 38)[25,29]. Whereas when the device was illuminated with light from a solar

simulator (1.5 solar mass) with increasing light intensity, different I-V responses were observed. In (Figure 39), an increase in current while there is an increase in light intensity shows the electron conduction pathway through ZnO nanorods because of the photosensitivity of ZnO. To further confirm that the photocurrent comes from ZnO, control experiments were done by illuminating only Au nanoparticle arrays and illuminating the hybrid device via a long pass filter of 420 nm. No photo response was observed in either case, which indicates UV light is required for the excitation of ZnO and thus generate the photocurrent.

Modulation on the I-V response compose of two pathways, the Au nanoparticle array pathway that follows power law dependence and ZnO pathway (schematic in Figure 28) which obeys a Schottky equation[27]. The overall equation fits the I-V response of the hybrid device (equation 4).

$$I = P_1[exp(P_2V)] + k\left(\frac{V}{V_T} - 1\right)^{\alpha} \quad (4)$$

In equation 4, the Schottky current that pass though the Au electrode to ZnO nanorods to another Au electrode is represented in the first term. P_1 is the saturation current and it is also relate to the thermionic emission over the barrier. P_2 combines thermal energy, electron charge and the ZnO ideality factor.

The second term represents the power law for calculating current pass through the Au nanoparticle arrays. k characterizes the current through a

single nanoparticle channel in the pathway. V_T is the threshold voltage required for the electron to start passing through. α relates to the dimensionality of the nanoparticle array and is the scaling exponent.

By fitting this equation to the I-V response date of dark condition and under illumination in Figure 39, an accuracy of > 99% is produced. The effect of ZnO nanorods on Au nanoparticle arrays in the hybrid device is illustrated by the effect of light intensity on V_T & α in the power law. In theoretical models, α is ~ 5/3 for a typical 2-D arrays. Whereas α is in the range of 2 - 3.5 for electron conduction in 1-D single nanoparticle arrays because of local defects. A value of ~ 2.45 was observed in Figure 40 and corresponds to the fact of the Au nanoparticle arrays, which is a 2-D nanoparticles matrix with 1-D bottlenecks. These 1-D bottlenecks are due to the nature of the Ca-Au chains which form a 1-D structure. There is no significant change in α under different illumination conditions, as a result of the ZnO photo excitation not affecting dimensionality of the underlying Au nanoparticle arrays.

On the contrary, photo excitation of ZnO nanorods changes the threshold voltage significantly. Figure 40 shows the decrease in V_T upon illumination. The phenomenon is similar to gating on these arrays by an external electric field. As a semiconductor, electron-hole pairs are generated under illumination. The surface defects on the nanorods trap the holes, the holes thus leads to a local gating of Au nanoparticles which alter the threshold voltage on Au matrix. Further increasing the light intensity results

in a stabilization of the threshold voltage, which can be explained by the saturation of electron-hole pairs at high light intensity. A control experiment of gating effect was done by using only Au nanoparticle chains assembled by Ca^{2+} ions. When increasing gate voltage, a similar decrease in the threshold voltage is observed in inset of Figure 40.

To investigate the effect of the underlying Au nanoparticle arrays on photocurrent of ZnO nanorods, a set of constant bias were applied to the hybrid device. The responses were recorded in Figure 41, and a trend of increasing current with increasing bias can be seen from this figure. When electron transport thought the Au nanoparticles, there is a greater charging of the nanoparticles to sustain the electric current. Furthermore, the increased charging would result in a greater interaction with the holes trapped on the surface of the ZnO nanorods. By modulating of the decay of the photocurrent in the hybrid device after turning off the illumination, a bi exponential equation with two time constants T_1 and T_2 are fitted to the decays. In figure 4b the change in the decay time constants with increasing bias is plotted in fig 4b. Larger time constants, greater electron charging of the Au nanoparticles and increased interaction with the ZnO surface trapped holes were observed as the bias increases. Therefore an increase in the decay time is then expected.

The current goes through ZnO nanorods pathway was separated from the overall current response of the hybrid device. It is the blue curve with a maximum in relative photocurrent at ~7 V in Figure 43. The black curve

shows the net relative photocurrent through the device increases with applied bias and stabilizes at higher voltage. With increasing bias, the base current of the Schottky junction of ZnO nanorods increases, result in a reducing contribution from the current generated by photo excitation. A P_1 value of ~ $1.5 \cdot 10^{-12}$ ampere is generated by the fit of the Schottky equation. The barrier height Φ_B can be calculated using the expression for the saturation current $P_1 = AT^2\exp(-\Phi_B/kT)$. A is the Richardson constant (32 $Acm^{-2}K^{-2}$ for ZnO), T is the temperature (298 Kelvin in our experiments) and k is the Boltzmann's constant. With a typical device area of 10 μm^2, the barrier height is calculated to be 0.67 eV. The value matches well with the literature values for Au-ZnO contacts. Figure 44 illustrates the relative current in the two pathways of ZnO nanorods and Au nanoparticle arrays in dark and under illuminations. When the bias is lower than the threshold voltage or close to it, ZnO nanorods pathway is the dominant electron conduction pathway. Au nanoparticle array becomes the dominant conduction pathway when the bias is in the range of 3-4 V and the hybrid device is in dark. Current contributed by ZnO nanorods recovers slowly at even higher biases. Therefore, the performance of the hybrid device can be controlled by the bias and light illumination. The electron conduction pathway changes from one to another, or a hybrid of both for ZnO nanorods and Au nanoparticles.

5. Conclusion

5.1 Summary of Findings

From the I-V response of the hybrid device, characteristic behavior of Au nanoparticle arrays including Coulomb blockade at room temperature, single electron charging effects and a power law dependence were observed. Schottky behavior and photocurrent generation due to the ZnO nanorods were also proved. The hybrid system also has coupling between the Au nanoparticles and ZnO rods other than the individual characteristics, which can be seen from the modulation between two pathways.

In this study, a ZnO nanorod interface on Au nanoparticle arrays was fabricated, which results in the photo-modulation of the array characteristics. By electrodepositing ZnO on Au nanoparticle arrays, we found the use of such nanoparticle arrays as electrochemical systems with both structural and spatial confinement of the synthesized material. This ability of Au nanoparticle chains significantly expands their potential use in sensors, multifunctional materials, single electron transistors and nanoscale energy systems.

5.2 Future Research

In addition to n-type ZnO, other semiconducting materials such as p-type Cu_2O, energy storage materials such as MnO_2, catalytic materials such as Pt and biological systems such as cells and proteins can be interfaced with these

arrays. These will be useful in applications as nanoscale devices have specific features.

References

1. Winter, M.; Brodd, R. J. What are batteries, fuel cells, and supercapacitors? *Chem. Rev.* **2004**, *104*, 4245-4269.

2. Kötz, R.; Carlen, M. Principles and applications of electrochemical capacitors. *Electrochim. Acta* **2000**, *45*, 2483-2498.

3. Miller, J. R.; Simon, P. Materials science: Electrochemical capacitors for energy management. *Science* **2008**, *321*, 651-652.

4. Lewandowski, A.; Galinski, M. Practical and theoretical limits for electrochemical double-layer capacitors. *J. Power Sources* **2007**, *173*, 822-828.

5. Burke, A. Ultracapacitors: Why, how, and where is the technology. *J. Power Sources* **2000**, *91*, 37-50.

6. Bélanger, D.; Brousse, T.; Long, J. W. Manganese oxides: Battery materials make the leap to electrochemical capacitors. *Electrochemical Society Interface* **2008**, *17*, 49-52.

7. Toupin, M.; Brousse, T.; Bélanger, D. Charge storage mechanism of MnO 2 electrode used in aqueous electrochemical capacitor. *Chemistry of Materials* **2004**, *16*, 3184-3190.

8. Beaudrouet, E.; Le Gal La Salle, A.; Guyomard, D. Nanostructured manganese dioxides: Synthesis and properties as supercapacitor electrode materials. *Electrochim. Acta* **2009**, *54*, 1240-1248.

9. Yu, M.; Sun, H.; Sun, X.; Lu, F.; Wang, G.; Hu, T.; Qiu, H.; Lian, J. Hierarchical al-doped and hydrogenated ZnO nanowire@MnO2 ultra-thin nanosheet core/shell arrays for high-performance supercapacitor electrode. *International Journal of Electrochemical Science* **2013**, *8*, 2313-2329.

10. Zilong, W.; Zhu, Z.; Qiu, J.; Yang, S. High performance flexible solid-state asymmetric supercapacitors from MnO2/ZnO core-shell nanorods//specially reduced graphene oxide. *Journal of Materials Chemistry C* **2014**, *2*, 1331-1336.

11. Reddy, A. L. M.; Gowda, S. R.; Shaijumon, M. M.; Ajayan, P. M. Hybrid nanostructures for energy storage applications. *Adv Mater* **2012**, *24*, 5045-5064.

12. Guo, Y. -.; Hu, J. -.; Wan, L. -. Nanostructured materials for electrochemical energy conversion and storage devices (Advanced Materials (2008) 20 (2878-2887)). *Adv Mater* **2008**, *20*, 2878-2887.

13. Aricò, A. S.; Bruce, P.; Scrosati, B.; Tarascon, J. -.; Van Schalkwijk, W. Nanostructured materials for advanced energy conversion and storage devices. *Nature Materials* **2005**, *4*, 366-377.

14. Özgür, Ü; Alivov, Y. I.; Liu, C.; Teke, A.; Reshchikov, M. A.; Dogan, S.; Avrutin, V.; Cho, S. -.; Morko , H. A comprehensive review of ZnO materials and devices. *J. Appl. Phys.* **2005**, *98*, 1-103.

15. Fan, Z.; Lu, J. G. Zinc oxide nanostructures: Synthesis and properties. *Journal of Nanoscience and Nanotechnology* **2005**, *5*, 1561-1573.

16. Wang, Z. L. Zinc oxide nanostructures: Growth, properties and applications. *Journal of Physics Condensed Matter* **2004**, *16*, R829-R858.

17. Beinik, I.; Kratzer, M.; Wachauer, A.; Wang, L.; Lechner, R. T.; Teichert, C.; Motz, C.; Anwand, W.; Brauer, G.; Chen, X. Y.; Hsu, X. Y.; Djurišic, A. B. Electrical properties of ZnO nanorods studied by conductive atomic force microscopy. *J. Appl. Phys.* **2011**, *110*.

18. Xu, F.; Lu, Y.; Xie, Y.; Liu, Y. Controllable morphology evolution of electrodeposited ZnO nano/micro-scale structures in aqueous solution. *Materials and Design* **2009**, *30*, 1704-1711.

19. Xu, L.; Chen, Q.; Xu, D. Hierarchical ZnO nanostructures obtained by electrodeposition. *Journal of Physical Chemistry C* **2007**, *111*, 11560-11565.

20. Zhang, T.; Dong, W.; Keeter-Brewer, M.; Konar, S.; Njabon, R. N.; Tian, Z. R. Site-specific nucleation and growth kinetics in hierarchical nanosyntheses of branched ZnO crystallites. *J. Am. Chem. Soc.* **2006**, *128*, 10960-10968.

21. Xu, L.; Guo, Y.; Liao, Q.; Zhang, J.; Xu, D. Morphological control of ZnO nanostructures by electrodeposition. *J Phys Chem B* **2005**, *109*, 13519-13522.

22. Gogotsi, Y.; Simon, P. True performance metrics in electrochemical energy storage. *Science* **2011**, *334*, 917-918.

23. Stoller, M. D.; Ruoff, R. S. Best practice methods for determining an electrode material's performance for ultracapacitors. *Energy and Environmental Science* **2010**, *3*, 1294-1301.

24. Likharev, K. K. Single-electron devices and their applications. *Proc IEEE* **1999**, *87*, 606-632.

25. Middleton, A. A.; Wingreen, N. S. Collective transport in arrays of small metallic dots. *Phys. Rev. Lett.* **1993**, *71*, 3198-3201.

26. Muller, H.; Williams, D. A.; Mizuta, H. Coulomb blockade and disorder in 2D quantum dot arrays. *Jpn J Appl Phys Part 2 Letter* **2000**, *39*, L723-L725.

27. Müller, H. -.; Katayama, K.; Mizuta, H. Effects of disorder on the blockade voltage of two-dimensional quantum dot arrays. *J. Appl. Phys.* **1998**, *84*, 5603-5609.

28. Daniel, M. -.; Astruc, D. Gold Nanoparticles: Assembly, Supramolecular Chemistry, Quantum-Size-Related Properties, and Applications Toward Biology, Catalysis, and Nanotechnology. *Chem. Rev.* **2004**, *104*, 293-346.

29. Parthasarathy, R.; Lin, X. -.; Jaeger, H. M. Electronic transport in metal nanocrystal arrays: The effect of structural disorder on scaling behavior. *Phys. Rev. Lett.* **2001**, *87*, 1868071-1868074.

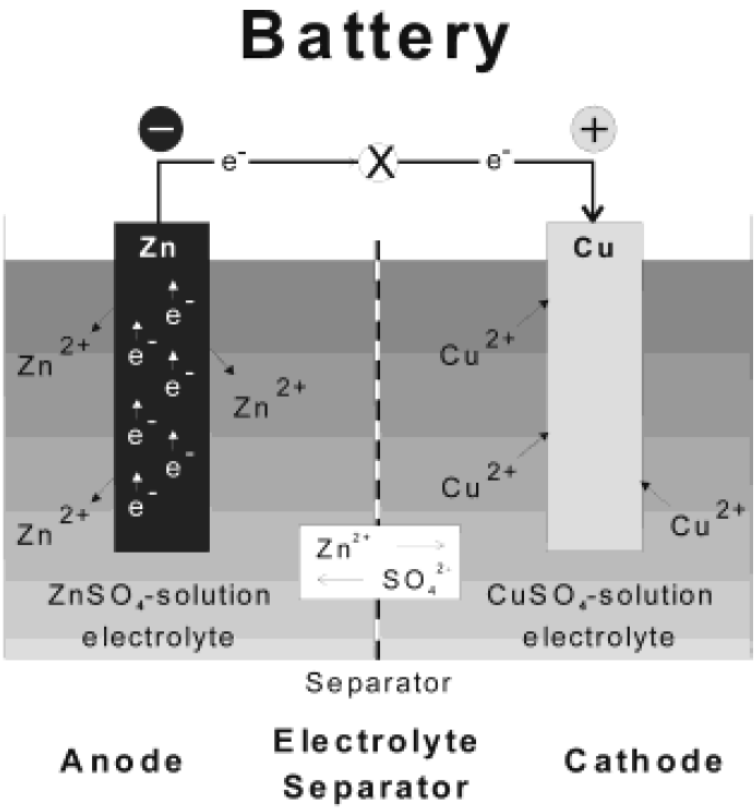

Figure 1. Schematic of a battery. (from Winter, M.; Brodd, R. J. 2004)

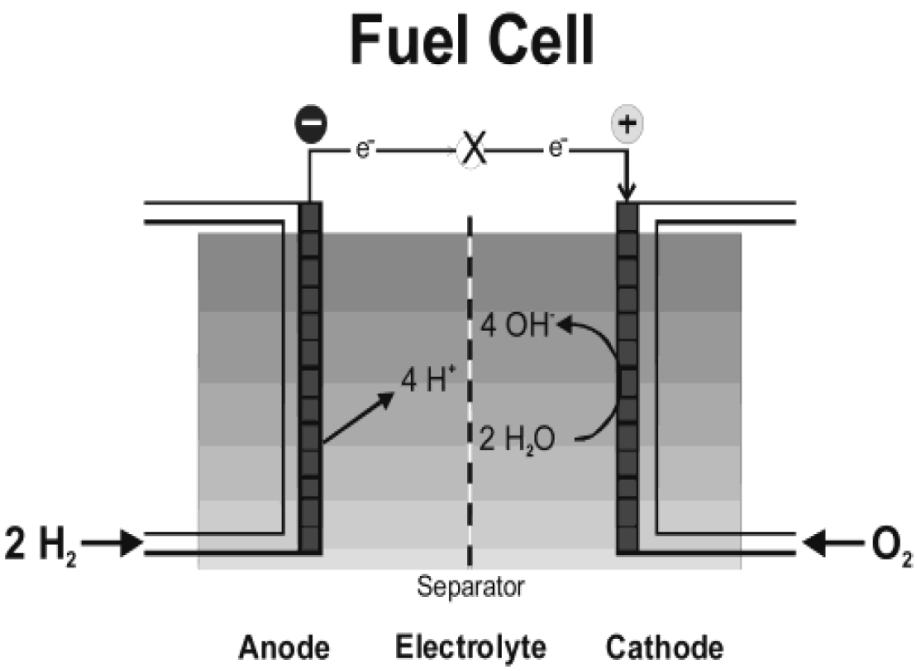

Figure 2. Schematic of a fuel cell. (from Winter, M.; Brodd, R. J. 2004)

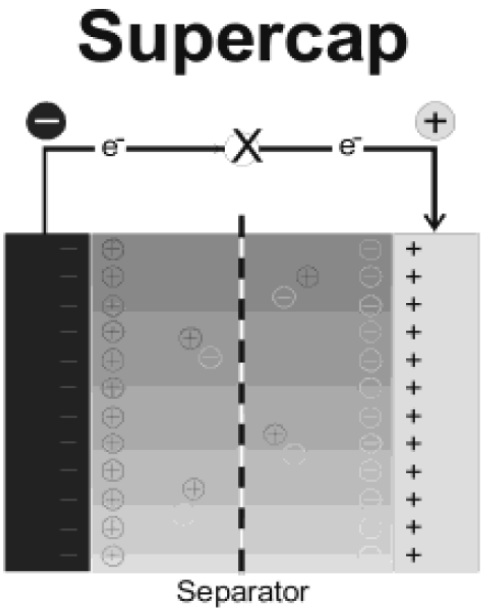

Figure 3. Schematic of a supercapacitor. (from Winter, M.; Brodd, R. J. 2004)

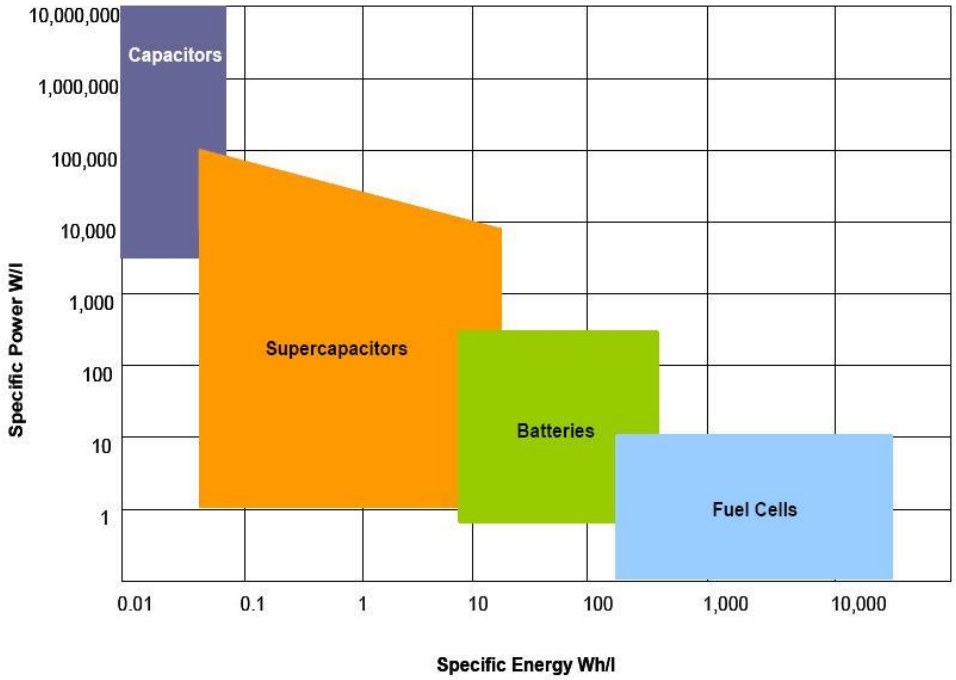

Figure 4. Comparison of energy density and power density for various energy storage devices. (from Hernandez, J. 2013)

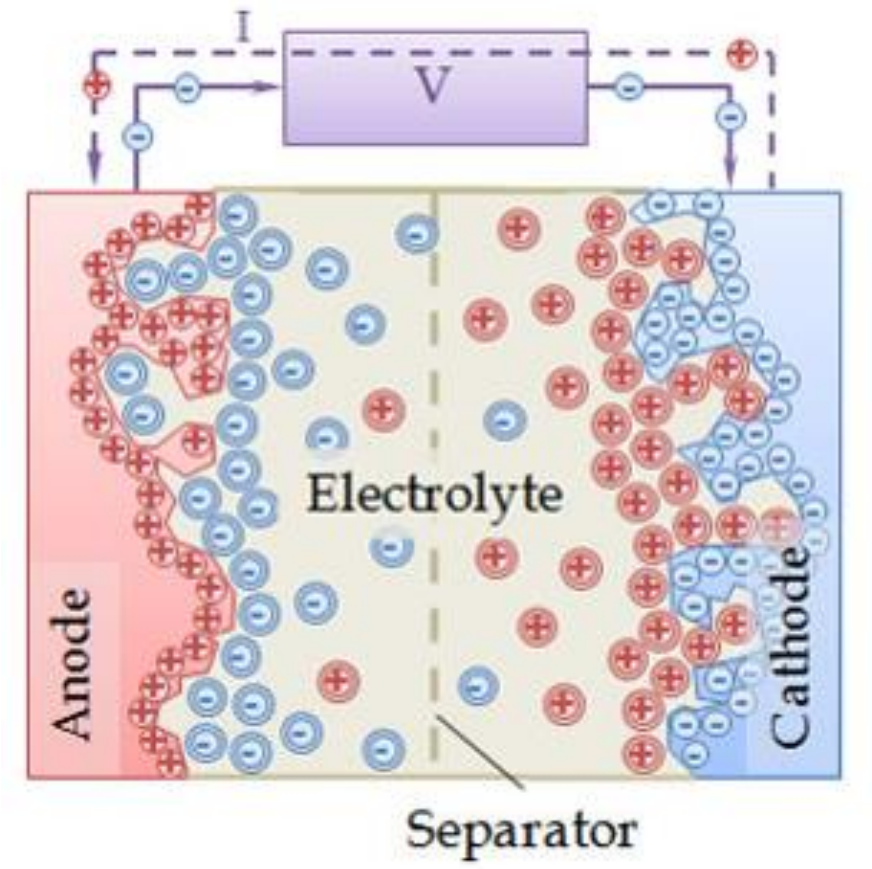

Figure 5. Schematic of an electric double-layer capacitor. (from Yu, A; Davies,A. 2011)

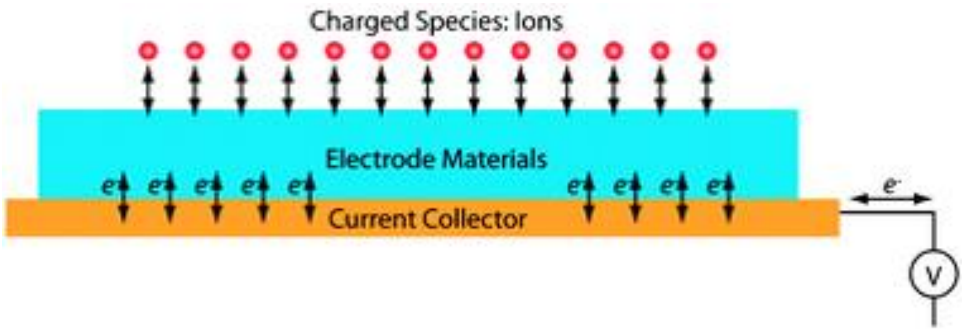

Figure 6. Schematic of charge transfer on the electrode of a pseudocapacitor. (from Liu, R; Duaya, W. 2009)

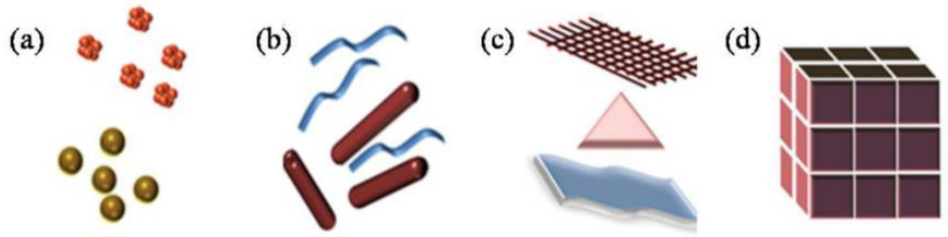

Figure 7. Examples of (a) 0-D nanomaterials, (b) 1-D nanomaterials, (c) 2-D nanomaterials and (d) 3-D nanomaterial. (from Alagarasi, A. 2011)

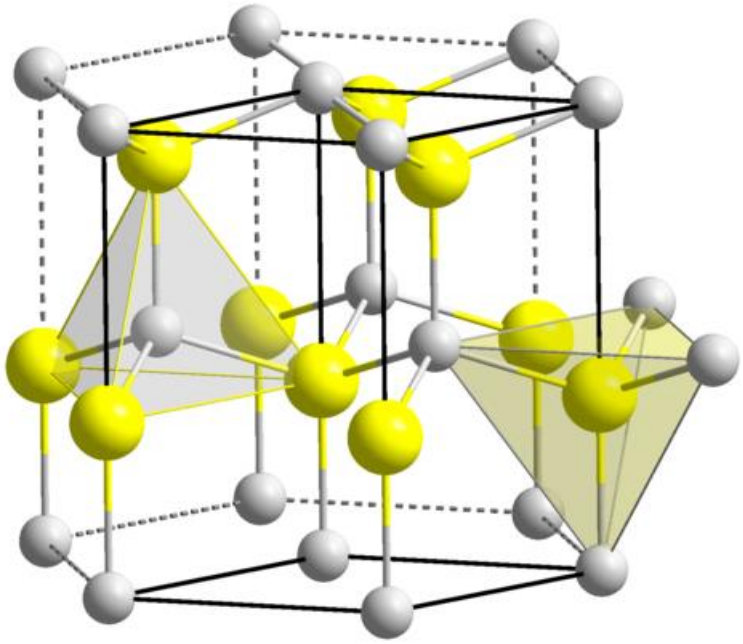

Figure 8. Wurtzite crystal structure. (from http://en.wikipedia.org/wiki/File:Wurtzite_polyhedra.png)

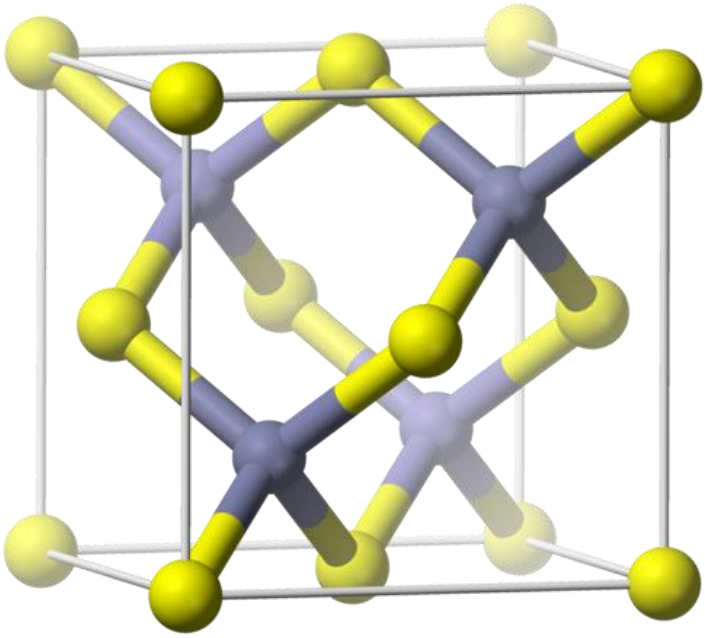

Figure 9. Zincblende crystal structure. (from http://en.wikipedia.org/wiki/File:Sphalerite-unit-cell-depth-fade-3D-balls.png)

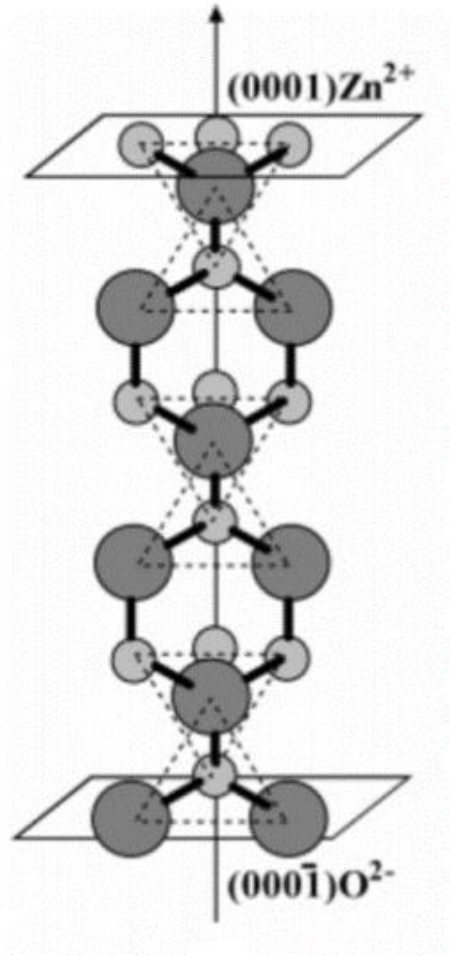

Figure 10. Top and basal surfaces in wurtzite crystal structure. (from Xu, L.; Guo, Y. 2005)

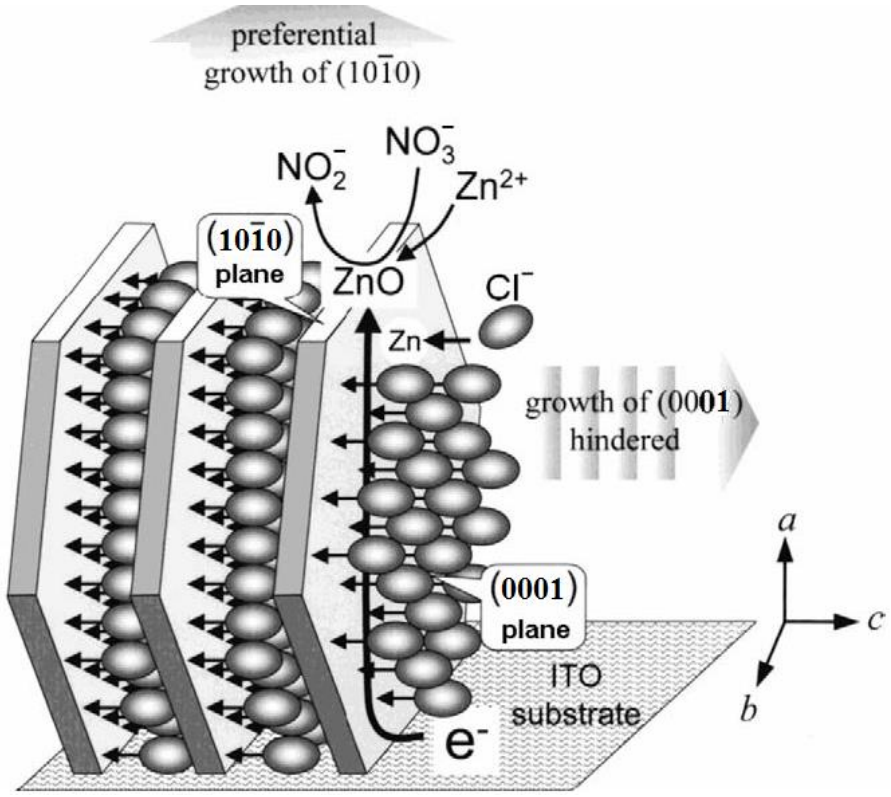

Figure 11. Preferential growth in other direction when the growth of (0001) plane is hindered by a capping agent. (from Xu, F.; Lu, Y. 2009)

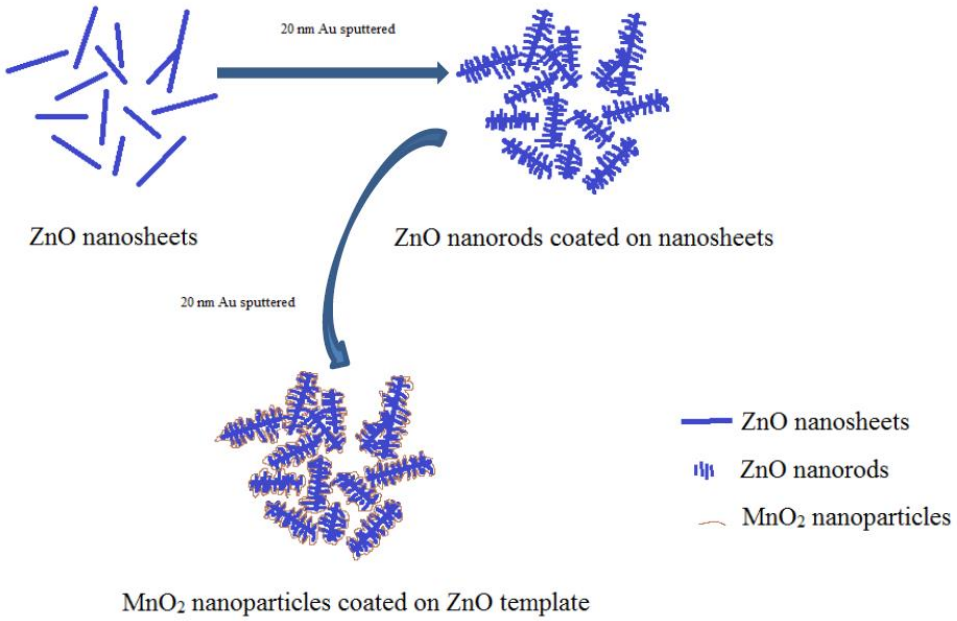

Figure 12. Scheme of the experiment.

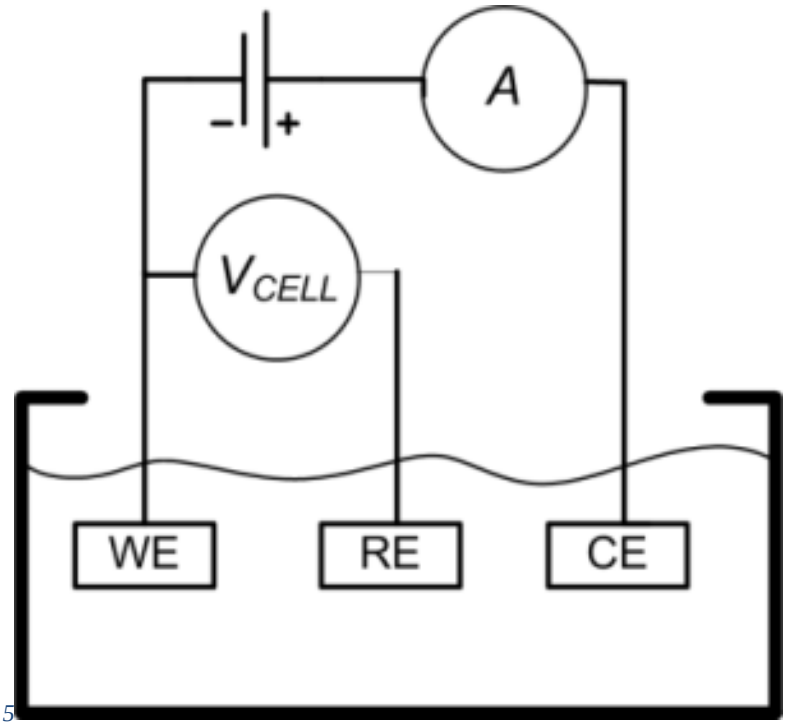

[5]

Figure 13. Schematic of a typical three-electrode setup.

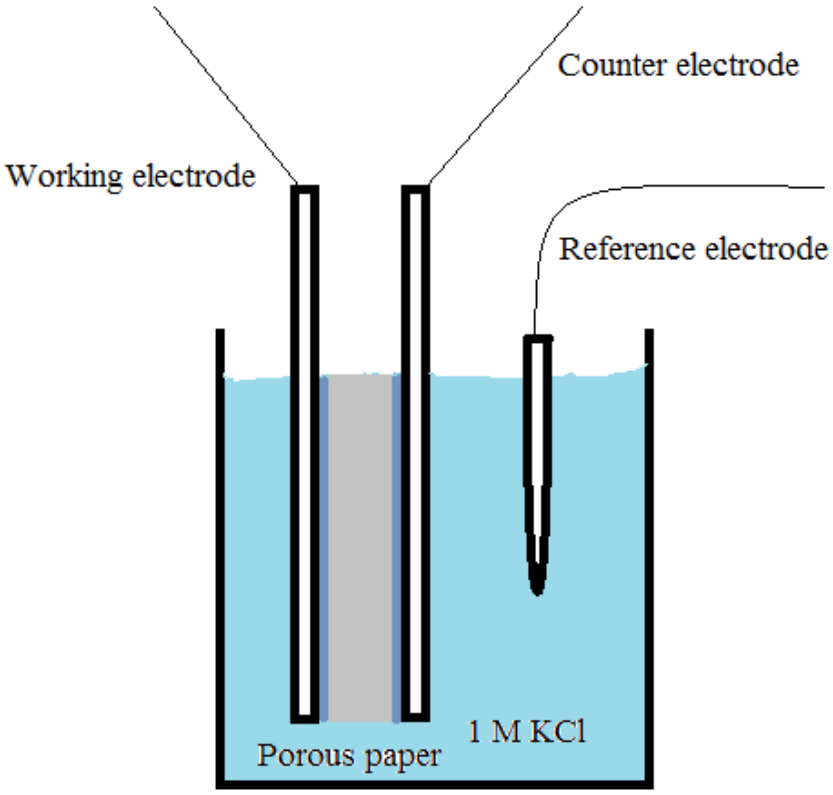

Figure 14. Schematic of test fixture configuration.

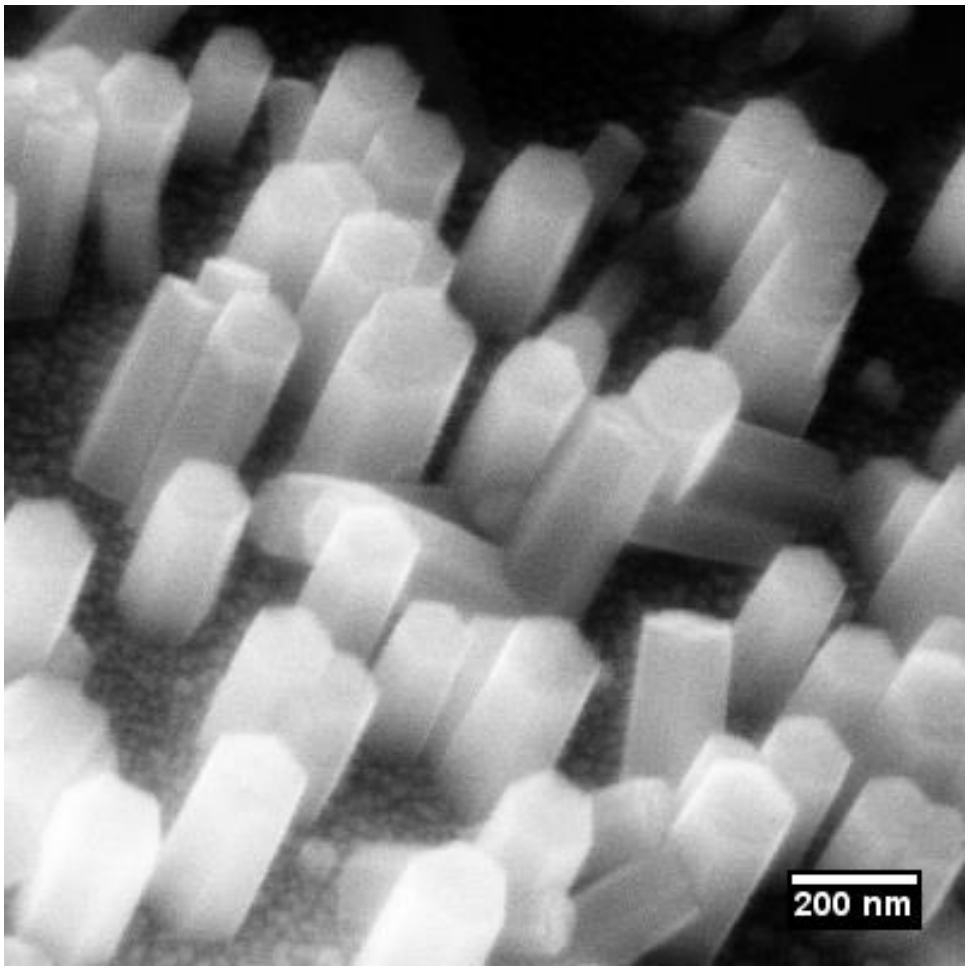

Figure 15. FE-SEM image of ZnO nanorods deposited in 0.005 M $Zn(NO_3)_2$.

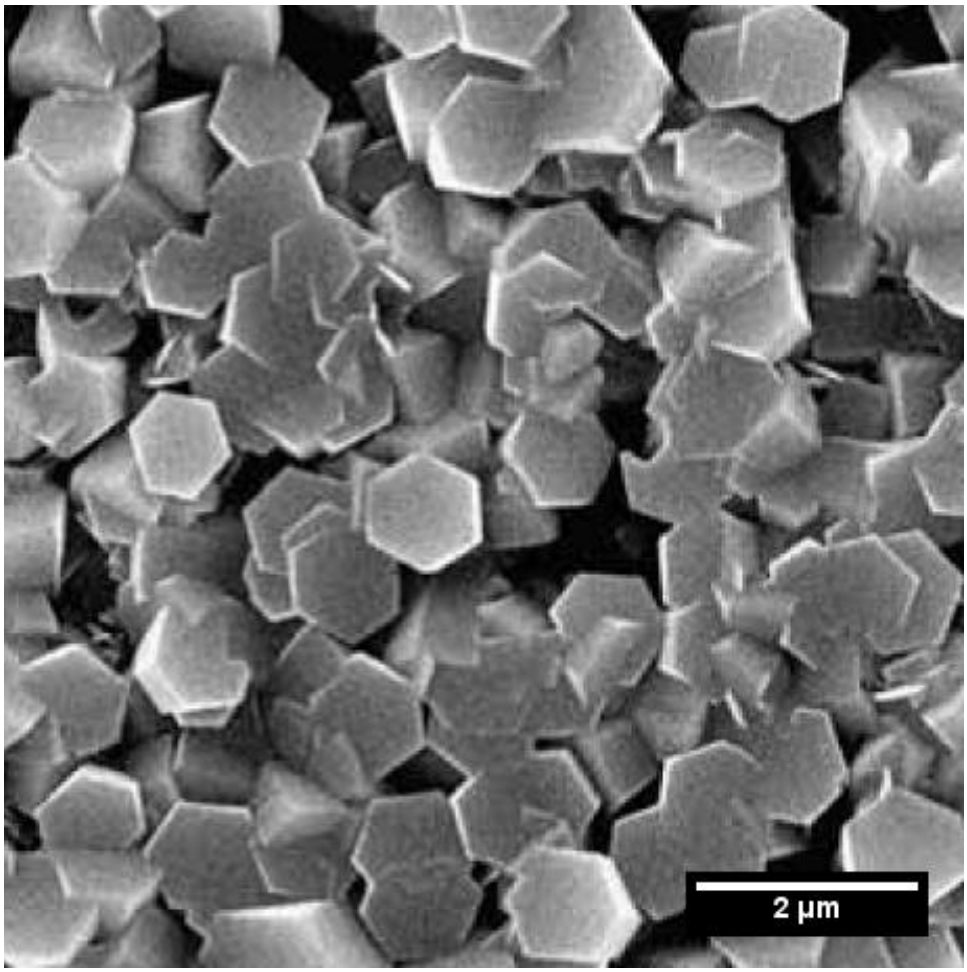

Figure 16. FE-SEM image of ZnO nanoplates deposited in 0.05 M $Zn(NO_3)_2$.

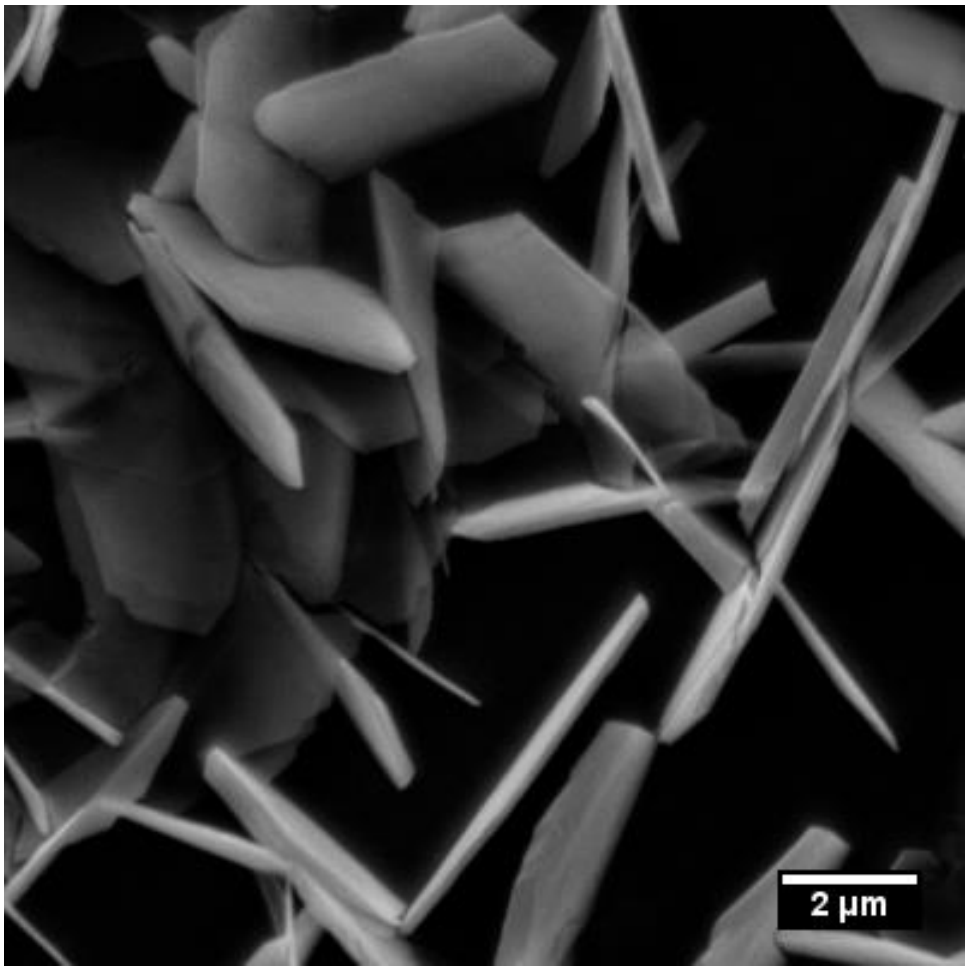

Figure 17. FE-SEM image of ZnO nanosheets deposited in 0.05 M $Zn(NO_3)_2$ and 0.06 M KCl.

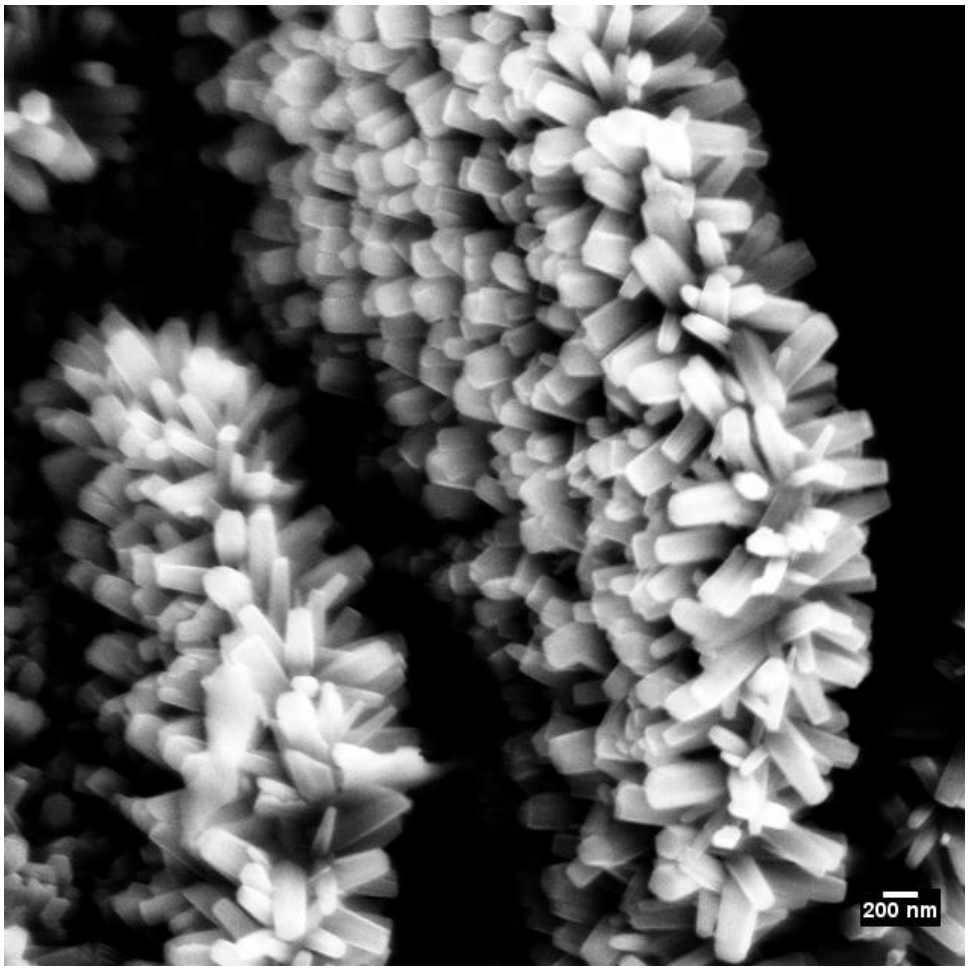

Figure 18. FE-SEM image of ZnO nanorods on ZnO nanosheets.

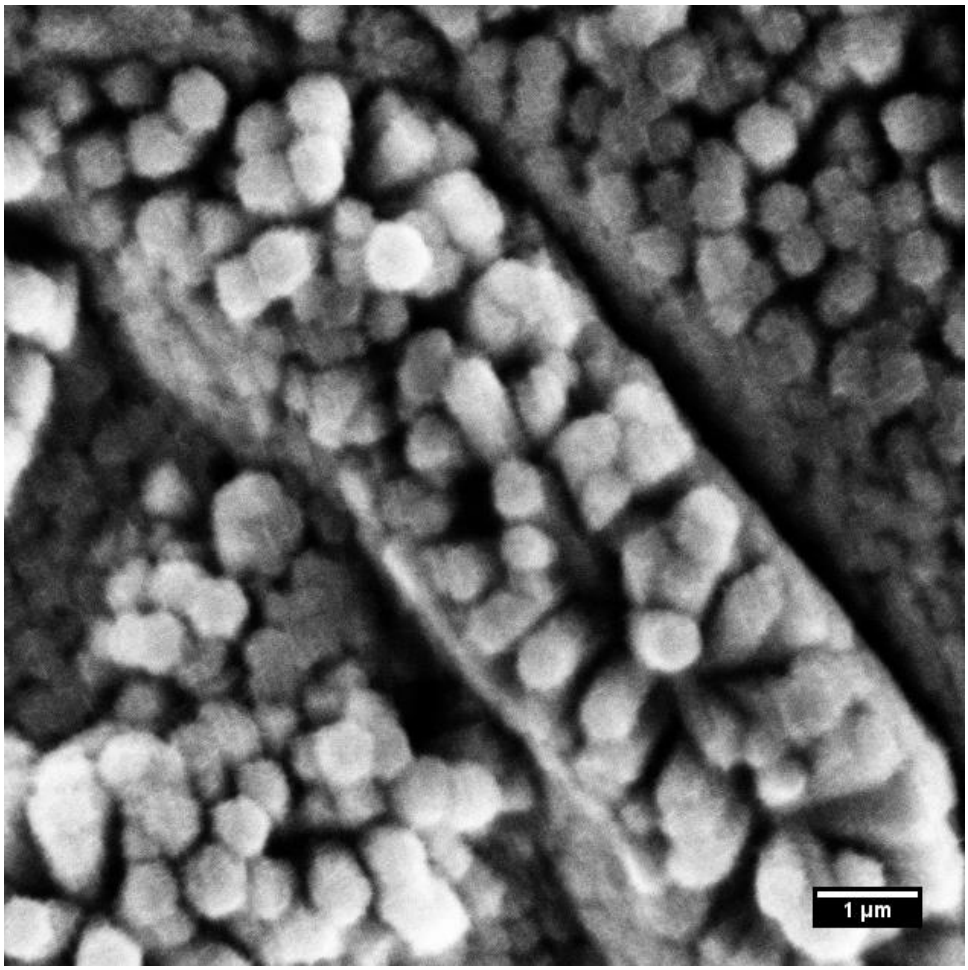

Figure 19. FE-SEM image of 5 minutes growth of MnO_2 on ZnO nanostructure.

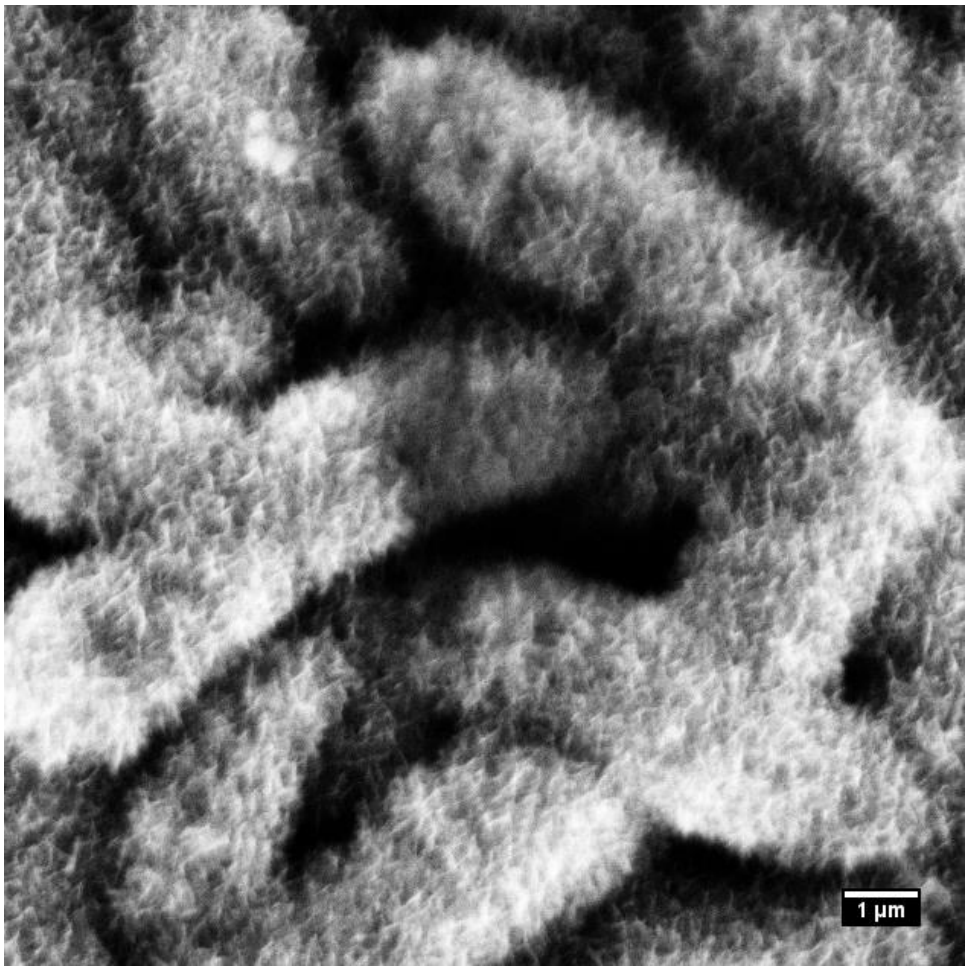

Figure 20. FE-SEM image of 20 minutes growth of MnO_2 on ZnO nanostructure.

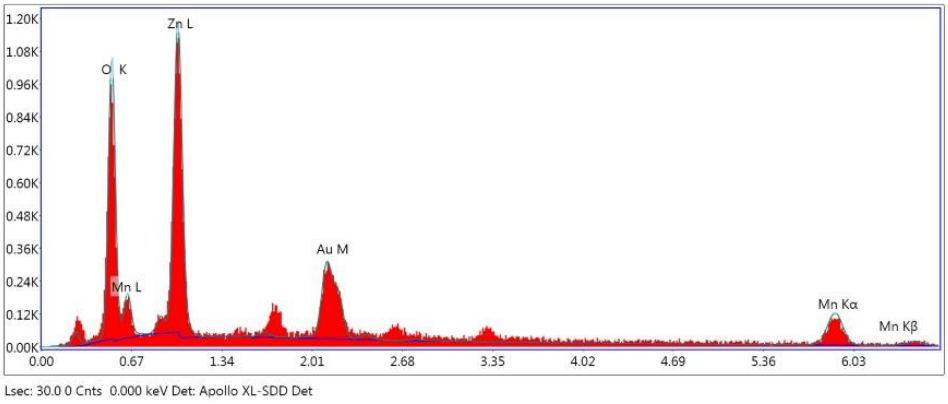

Figure 21. EDS spectrum of nanocomposite material.

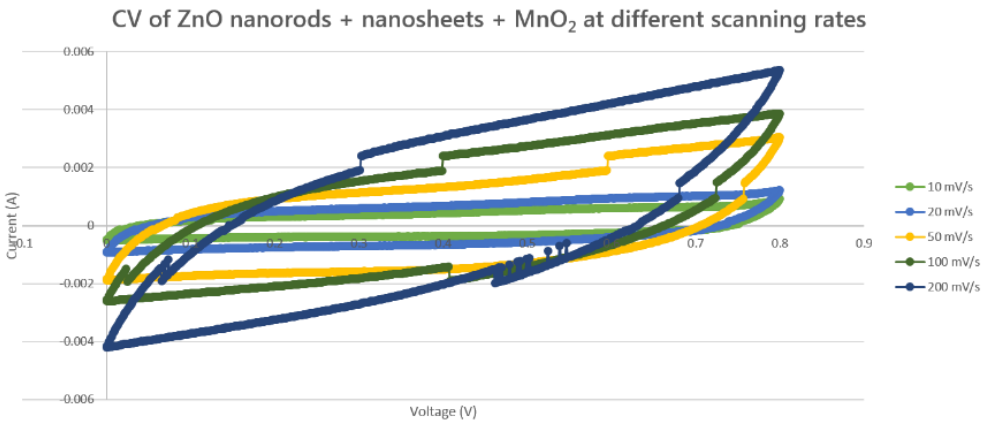

Figure 22. CVs of nanocomposite at different scan rates.

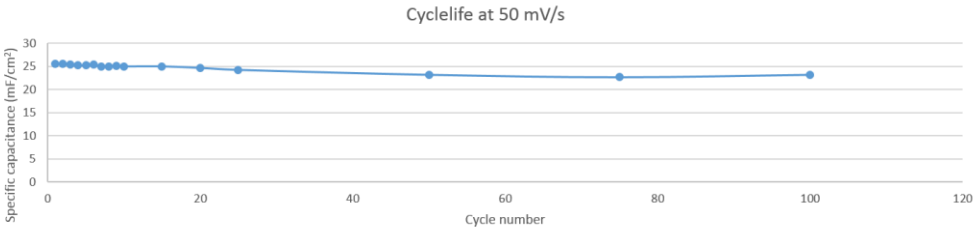

Figure 23. Cycle life of nanocomposite at 50 mV/s.

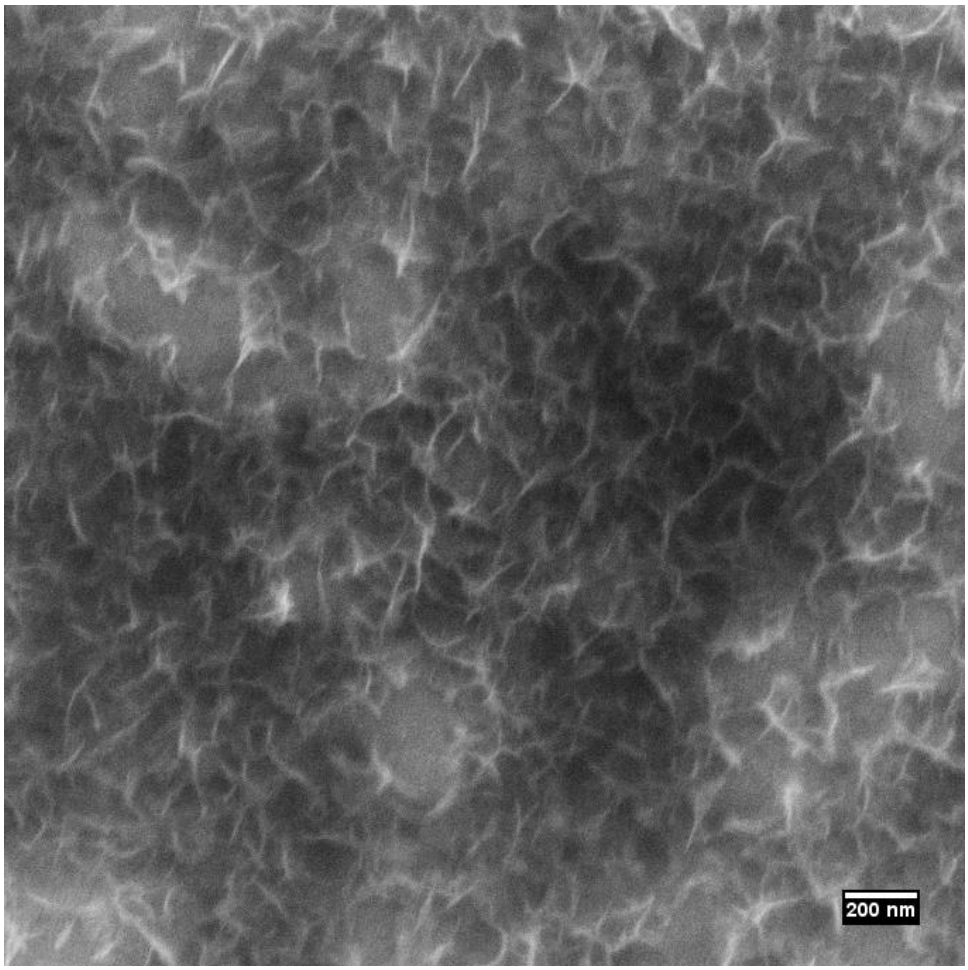

Figure 24. FE-SEM image of 5 minutes growth of MnO_2 on an ITO substrate.

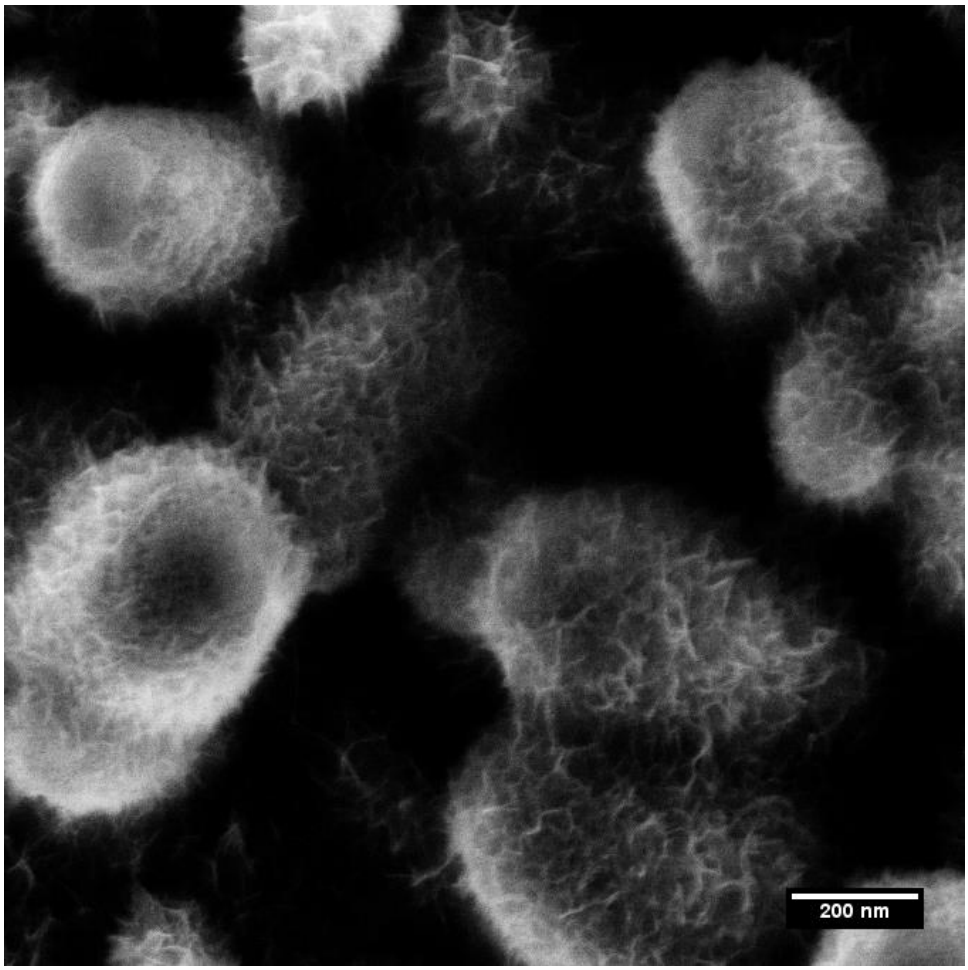

Figure 25. FE-SEM image of 5 minutes growth of MnO_2 on ZnO nanorods.

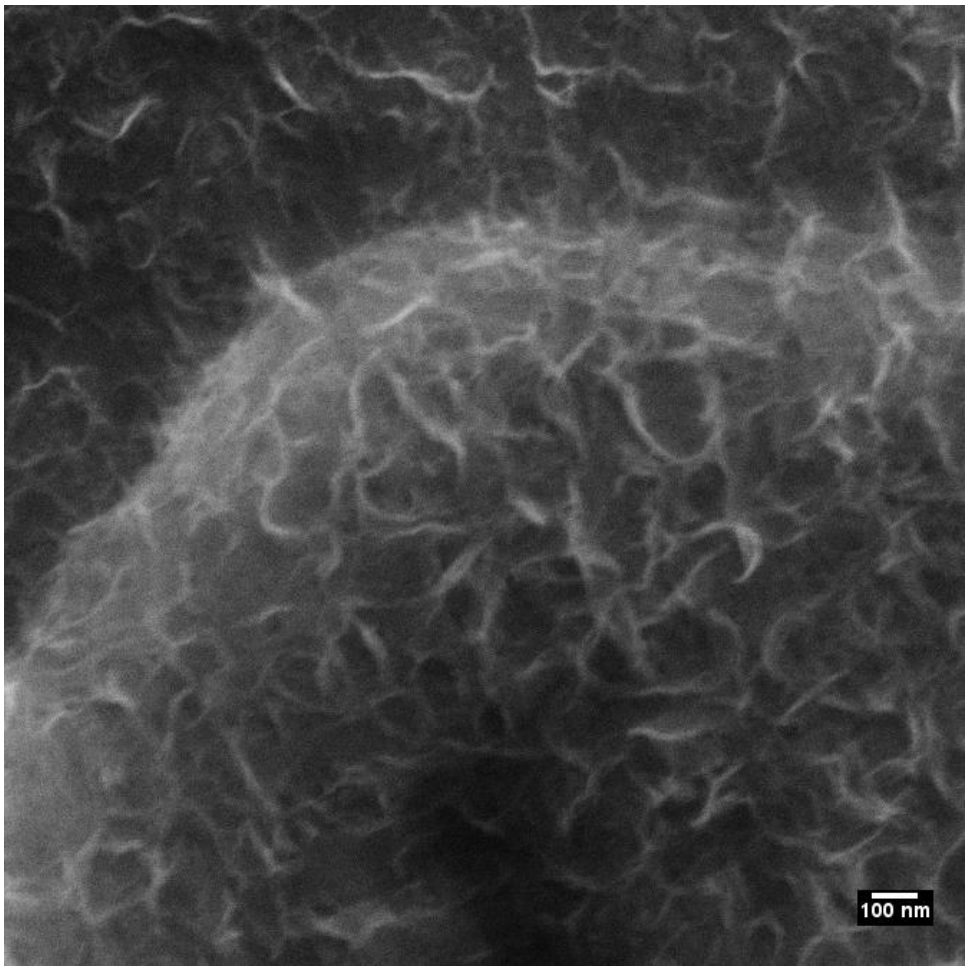

Figure 26. FE-SEM image of 5 minutes growth of MnO_2 on ZnO nanosheets.

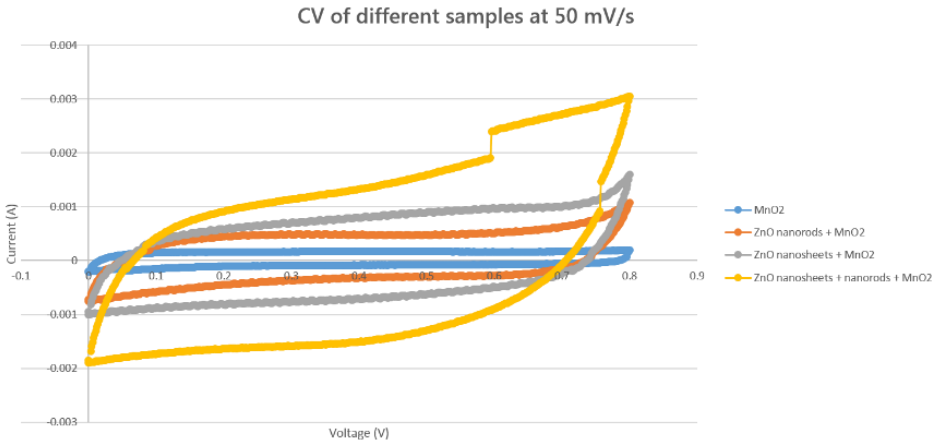

Figure 27. CVs of different samples at 50 mV/s.

Sample	MnO_2	ZnO nanorods + MnO_2	ZnO nanosheets + MnO_2	ZnO nanosheets + nanorods + MnO_2
Current Level (mA)	0.156	0.480	0.811	1.40
Specific Capacitance (mF/cm^2)	2.77	8.22	14.5	26.2

Table 1. Specific capacitance value of different samples.

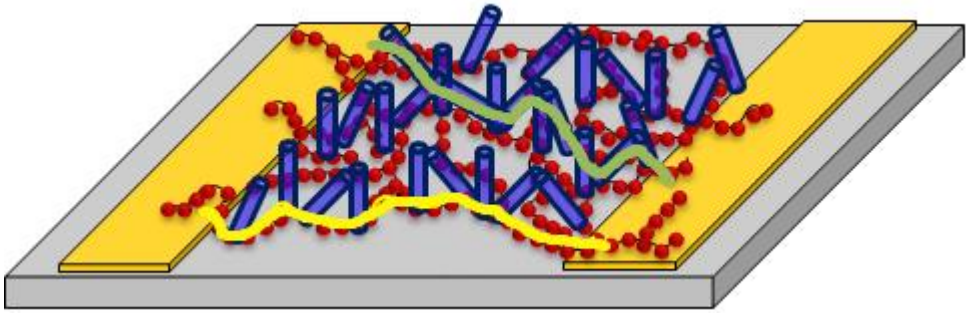

Figure 28. Schematic of the hybrid device of Au nanoparticle arrays and ZnO nanorods.

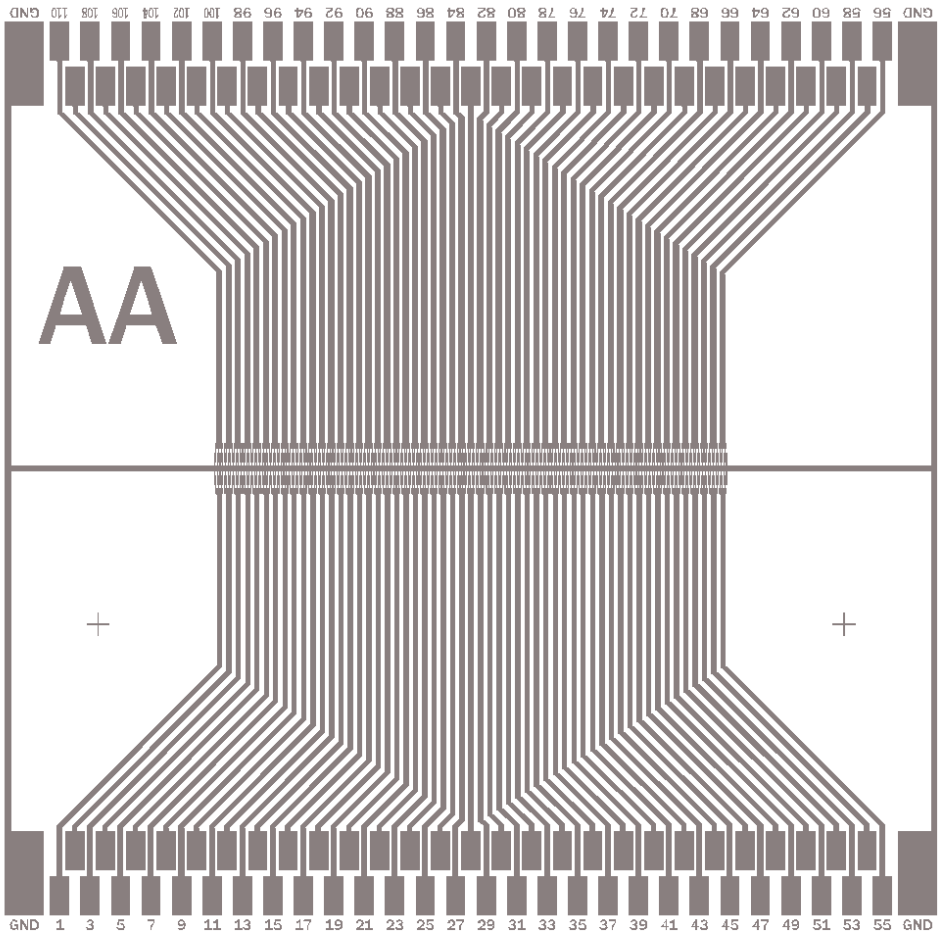

Figure 29.Schematic of a gold chip.

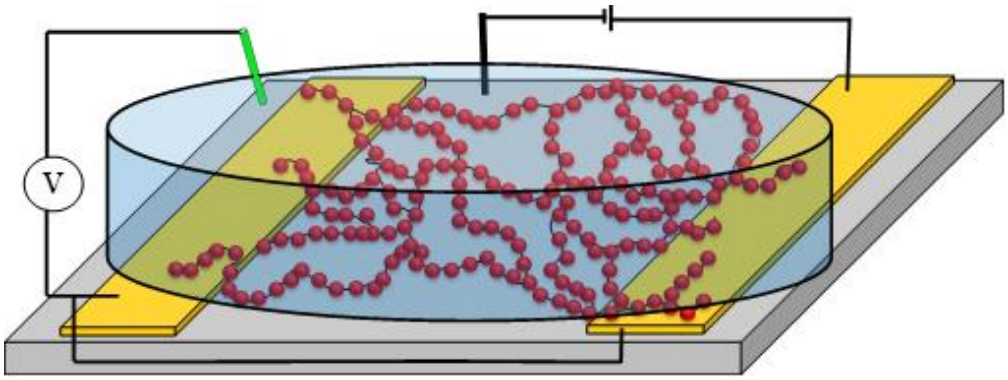

Figure 30. Schematic of electrodepositing ZnO on Au nanoparticle chains.

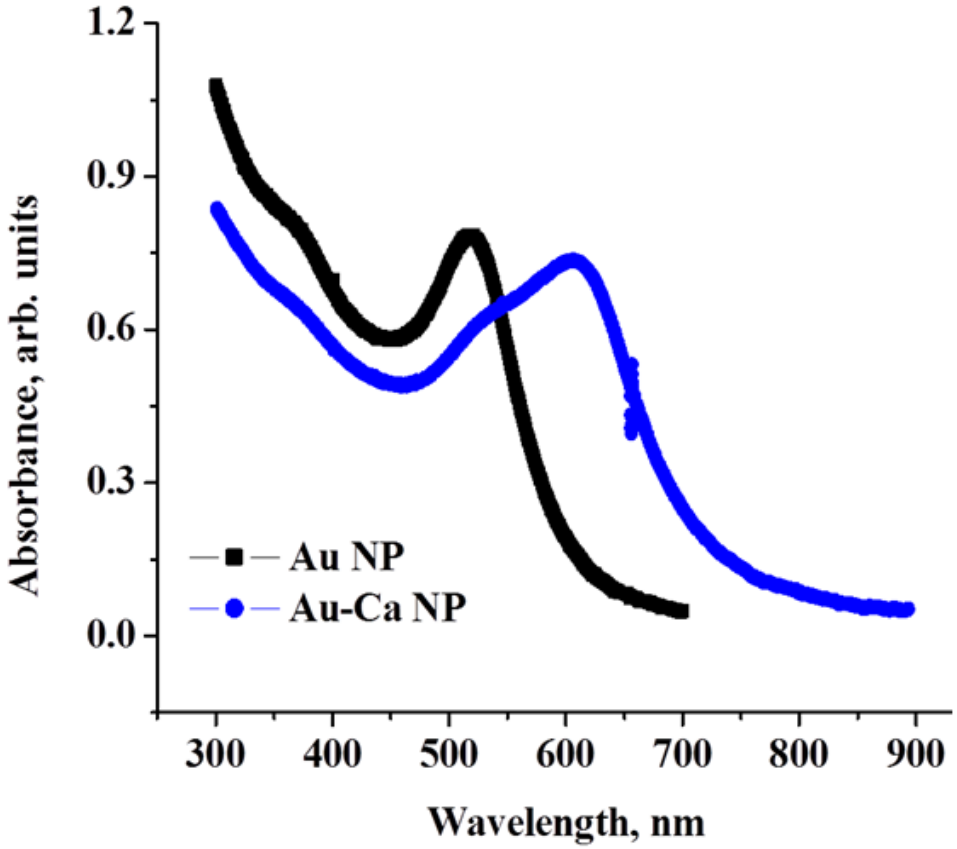

Figure 31.UV-Vis spectrum for Au and Au-Ca nanoparticles.

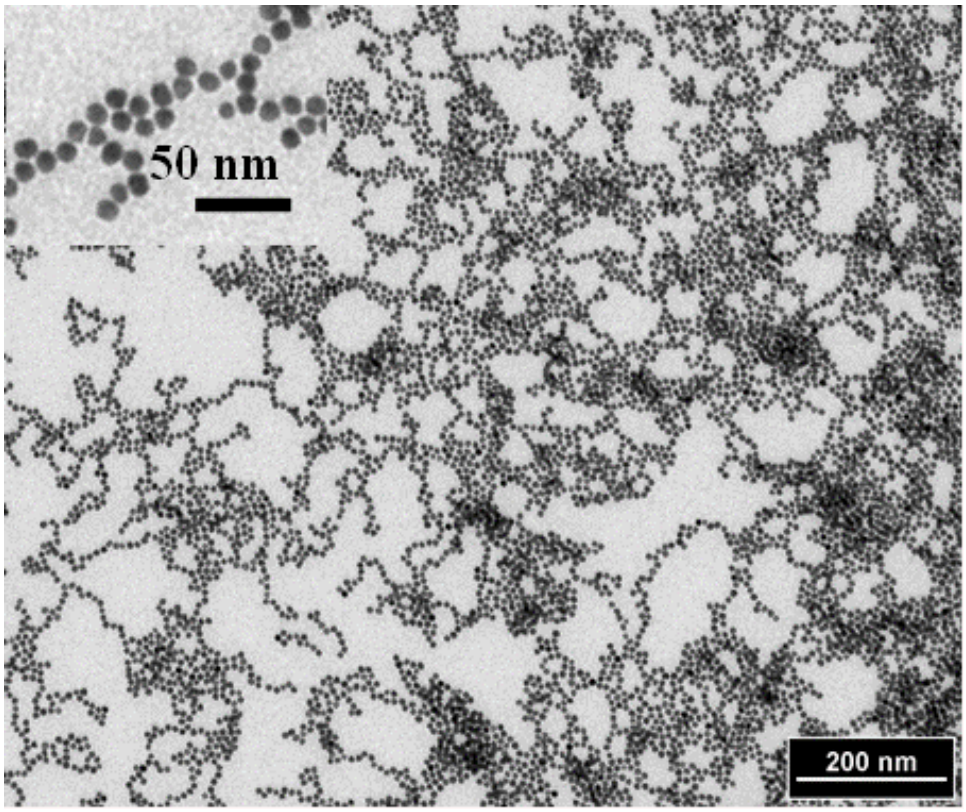

Figure 32. TEM image of Au nanoparticle arrays.

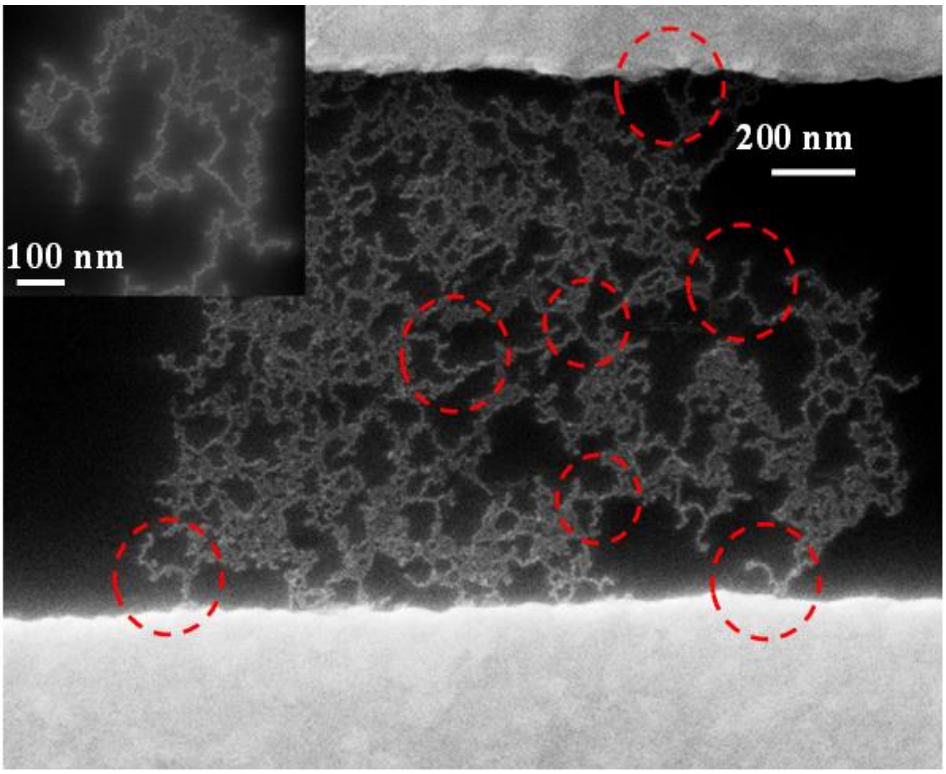

Figure 33. FE-SEM image of Au nanoparticle arrays connecting two electrodes.

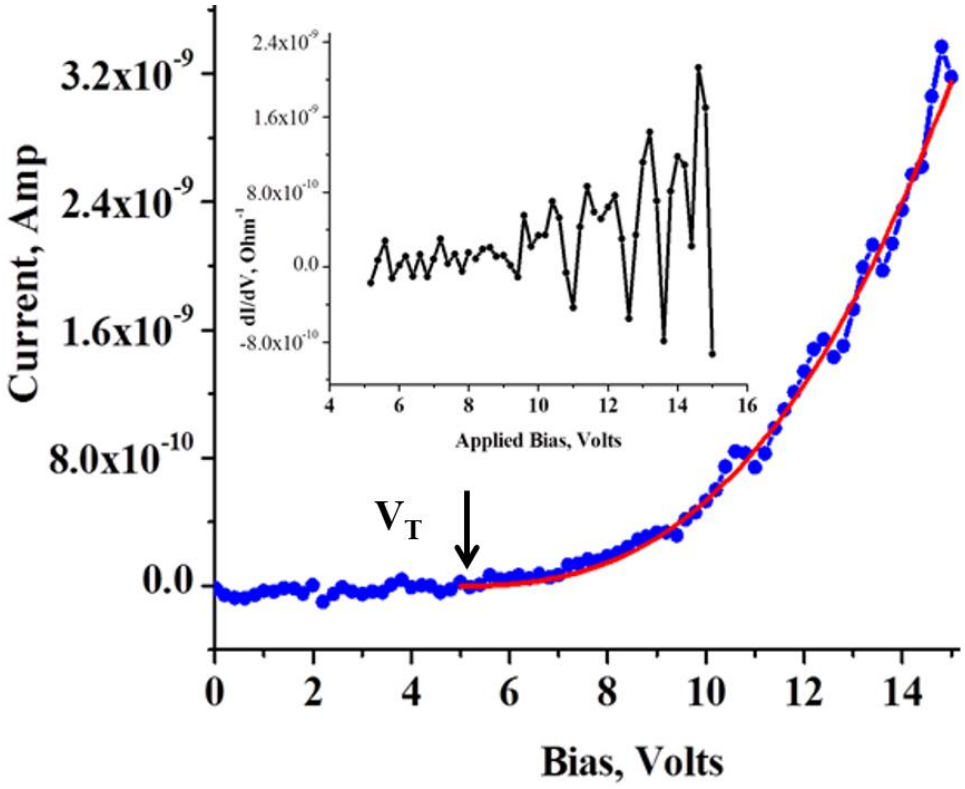

Figure 34. I-V response of Au nanoparticle arrays.

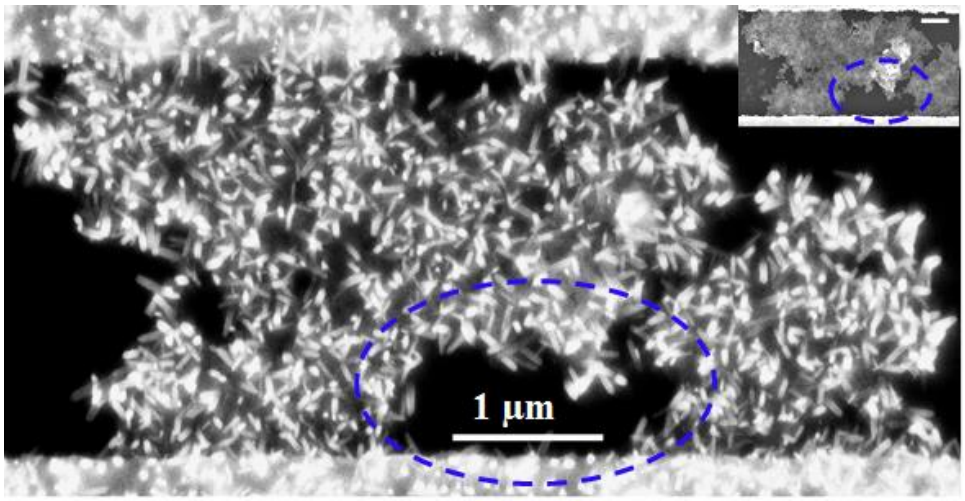

Figure 35. FE-SEM image of ZnO nanorods on Au nanoparticle chains.

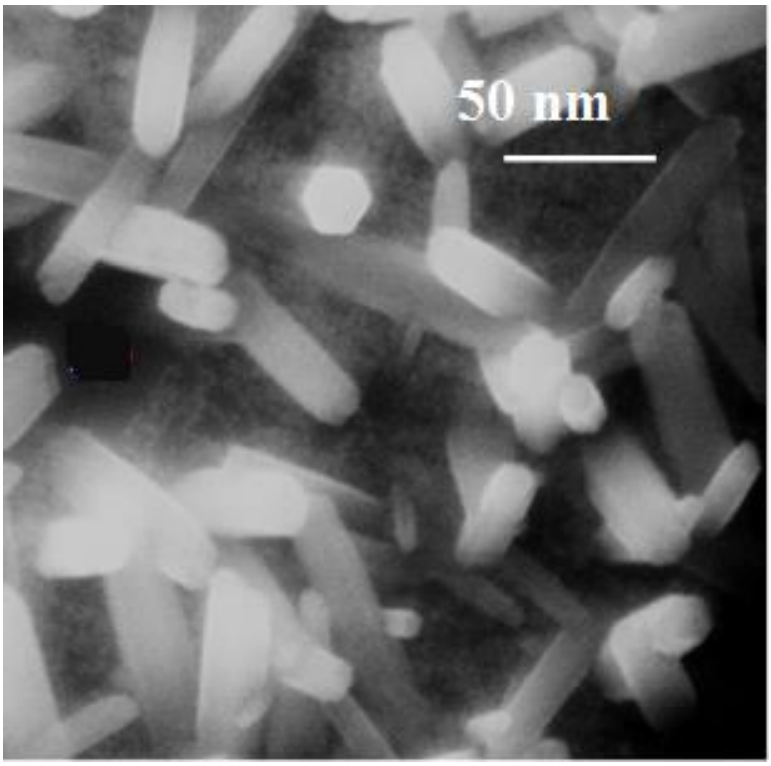

Figure 36. FE-SEM image of ZnO nanrods.

Figure 37. FE-SEM image of underlying Au nanoparticle arrays.

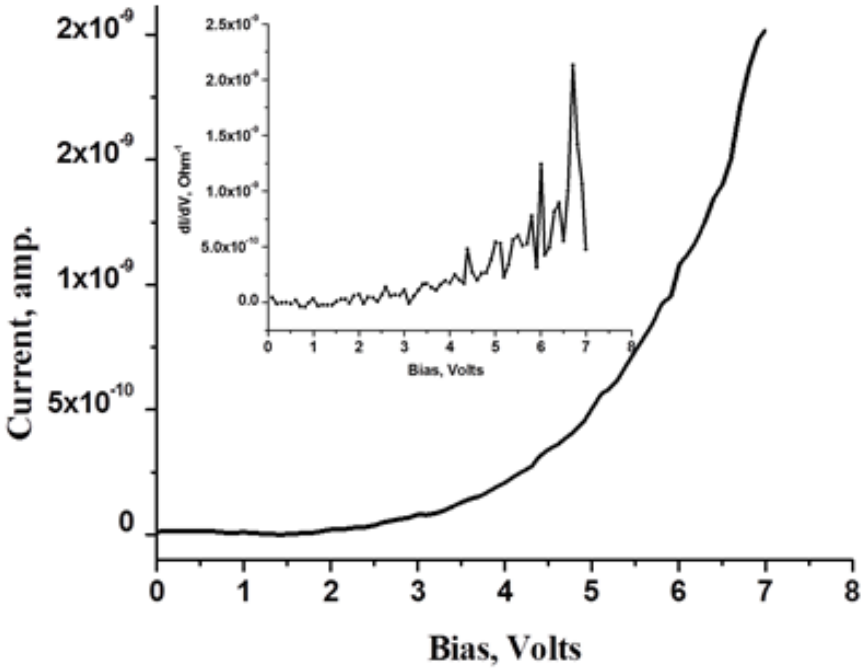

Figure 38. I-V response of the hybrid device under dark conditions.

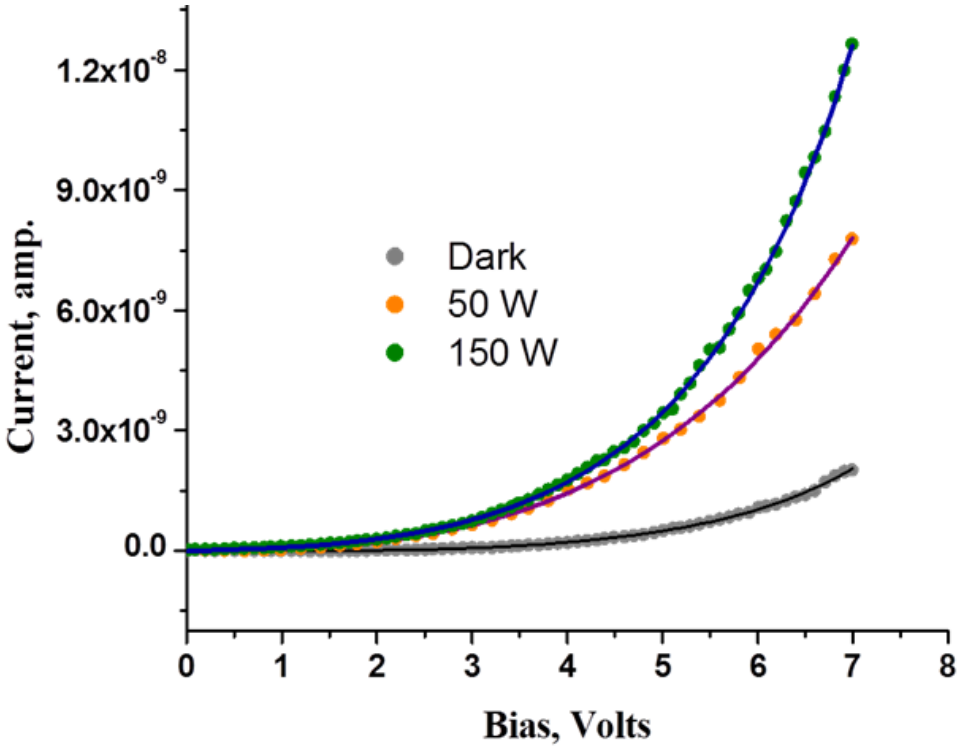

Figure 39. I-V responses of the hybrid devices under different light density.

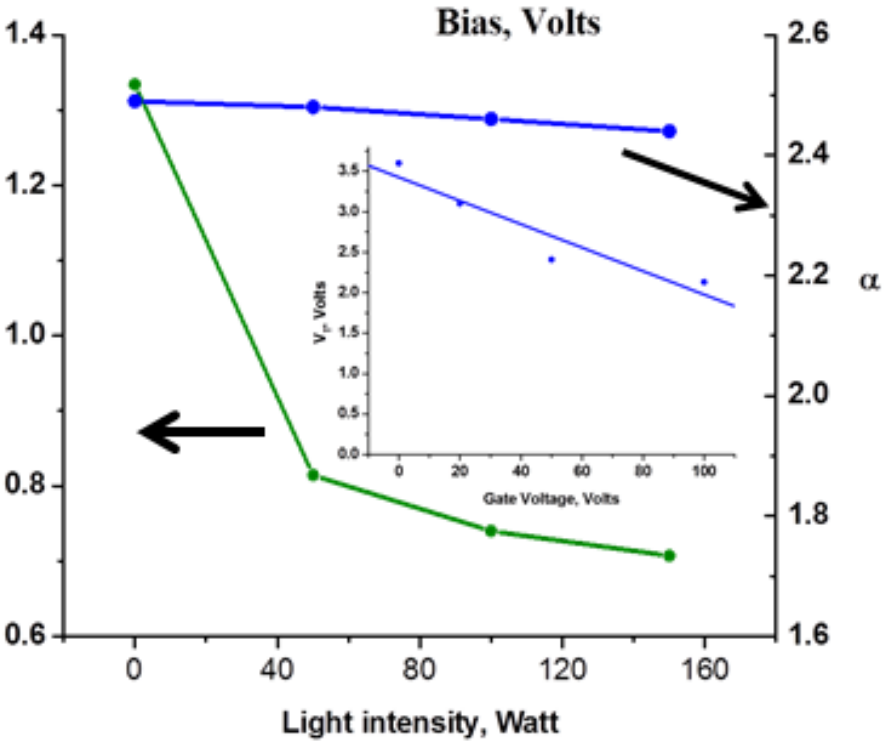

Figure 40. Effect of light intensity on the parameters V_T & α.

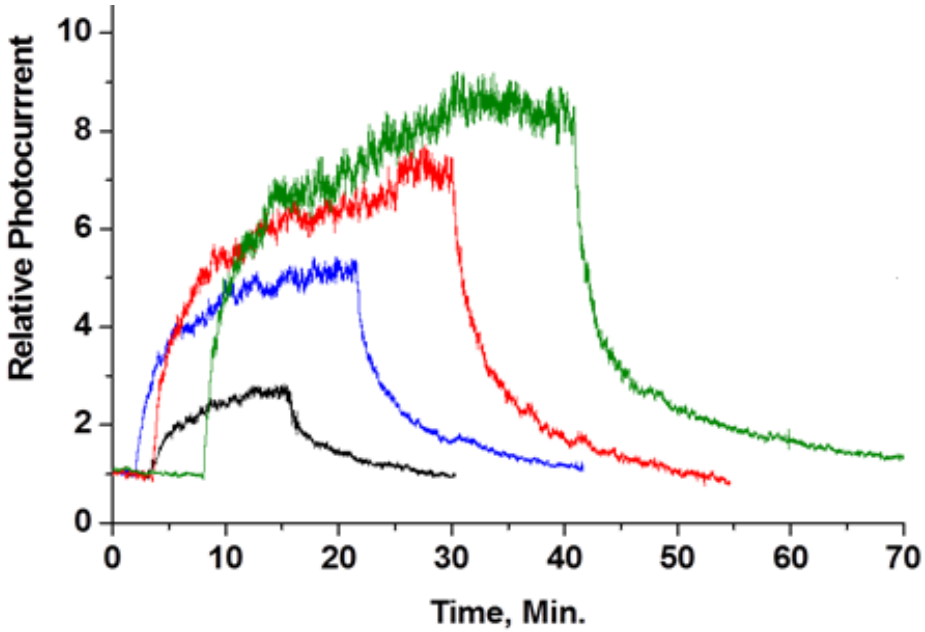

Figure 41. Net responses of photocurrent of the hybrid device at a series of constant bias.

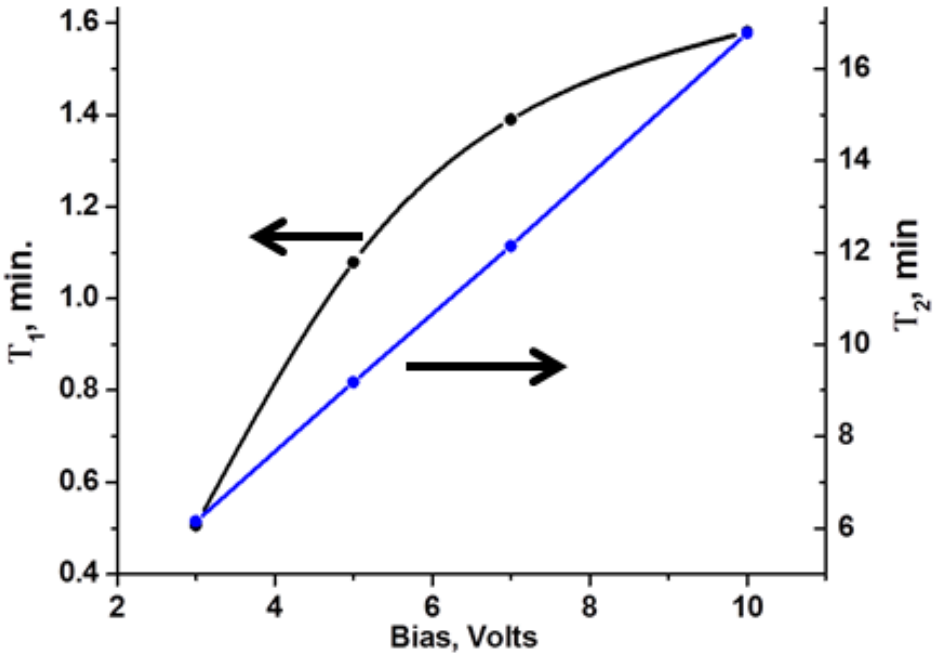

Figure 42. Change in the decay time constants with increasing bias to the hybrid device.

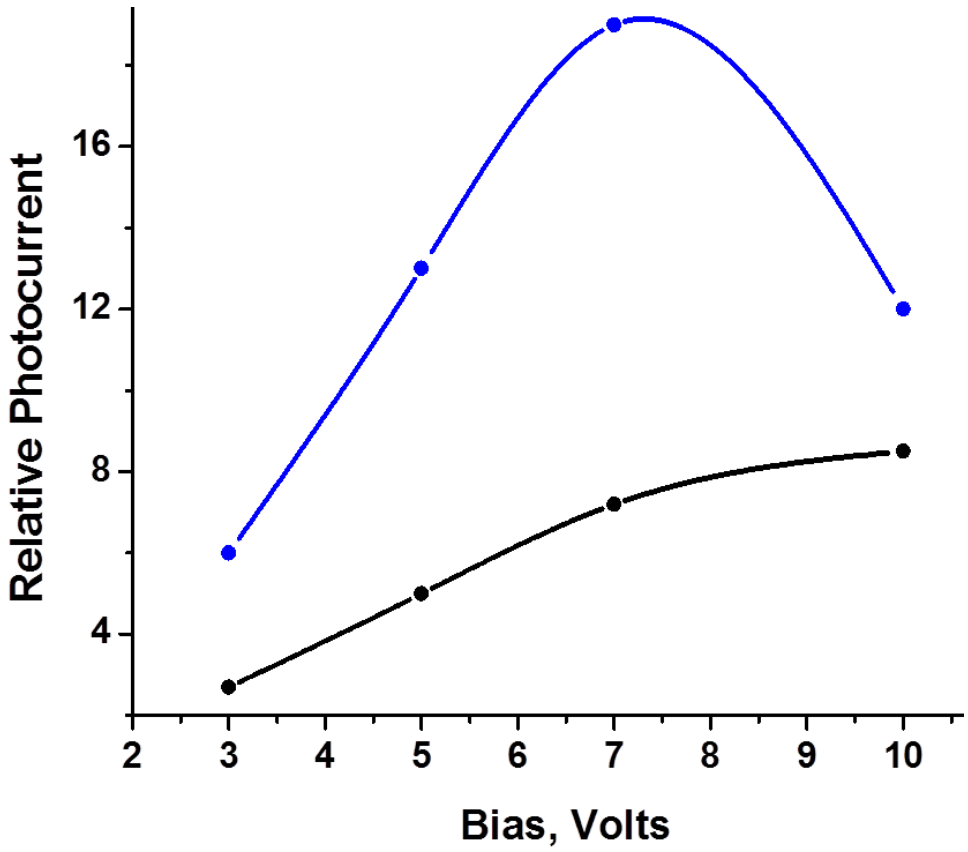

Figure 43. Decoupled photocurrent effect between Au nanoparticle chains and ZnO rods.

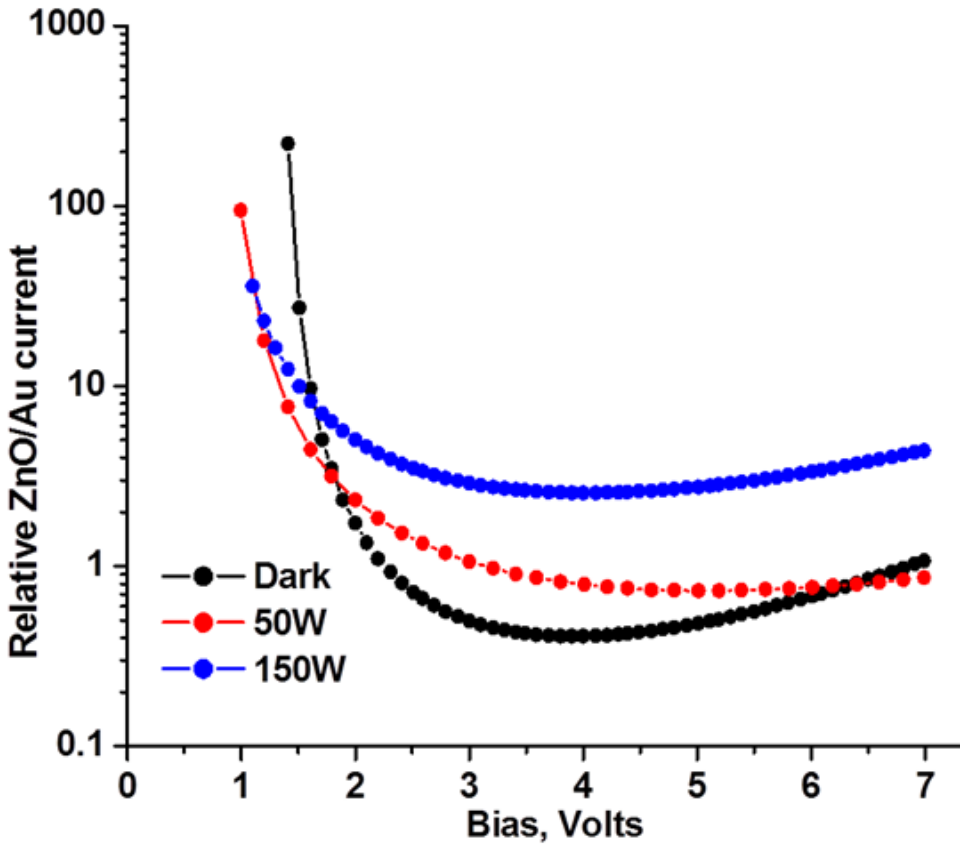

Figure 44. Relative current in two pathways of ZnO rods and Au nanoparticle arrays.